M2794.001800 MATERIAL AND MANUFACTURING PROCESSES

Chapter 3. Structural & Manufacturing Properties of Metals

Sung-Hoon Ahn

School of Mechanical and Aerospace Engineering
Seoul National University

Introduction

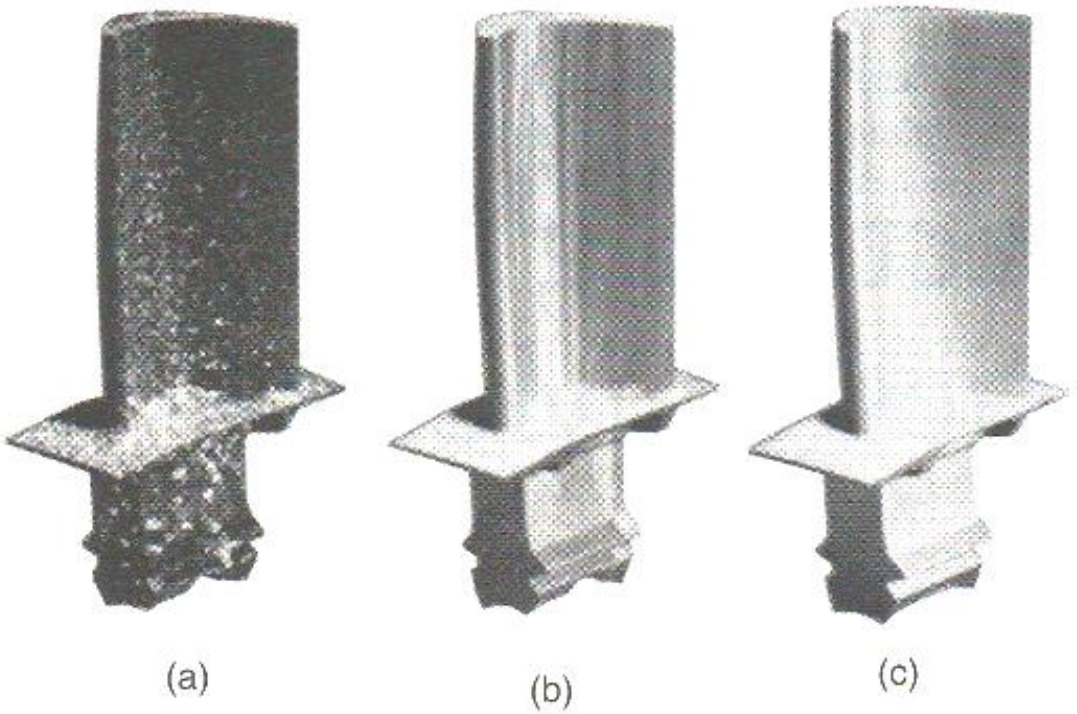

FIGURE 3.1 Turbine blades for jet engines, manufactured by three different methods: (a) conventionally cast; (b) directionally solidified, with columnar grains, as can be seen from the vertical streaks; and (c) single crystal. Although more expensive, single-crystal blades have properties at high temperatures that are superior to those of other blades. *Source:* Courtesy of United Technologies Pratt and Whitney.

Gas turbine

Periodic table (주기율표)

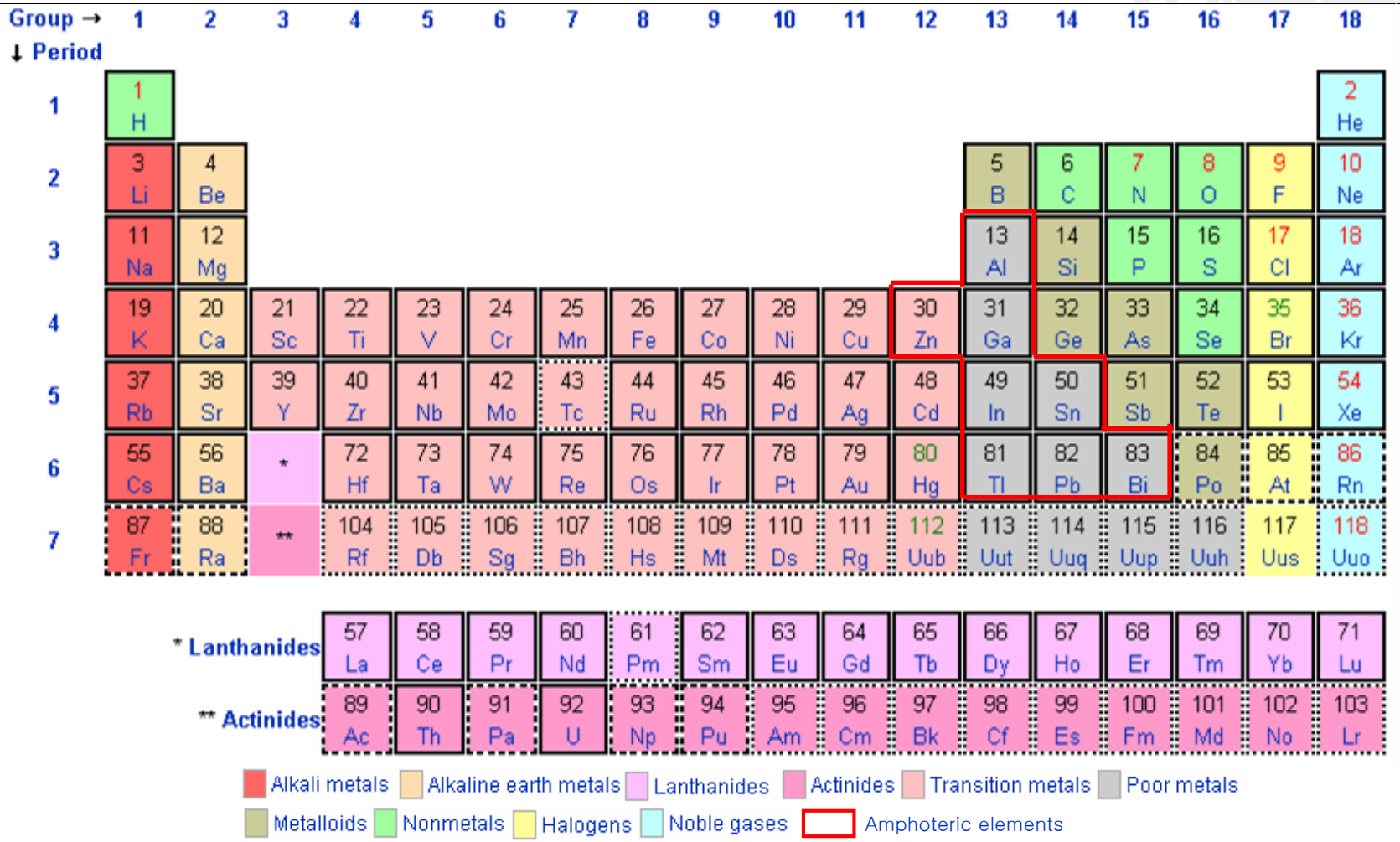

Metalloids(준금속) : the elements that are difficult to classify exclusively as metals or nonmetals and have properties between those of elements in the two classes

Amphoteric elements(양쪽성 원소) : the elements which have reactivity of a substance with both acids and bases, acting as an acid in the presence of a base and as a base in the presence of an acid.

Atomic bonds

- **Primary atomic bonds**
  - Ionic: attraction of positive & negative ions
  - Covalent: sharing of electrons
  - Metallic: free electron
- **Secondary atomic bonds**
  - van der Waals
  - Hydrogen bond

TABLE 2.3 Bonding Energies and Melting Temperatures for Various Substances

Bonding Type	*Substance*	*Bonding Energy*		*Melting Temperature* (°C)
		kJ/mol (kcal/mol)	*eV/atom, ion, molecule*	
Ionic	NaCl	640 (153)	3.3	801
	MgO	1000 (239)	5.2	2800
Covalent	Si	450 (108)	4.7	1410
	C (diamond)	713 (170)	7.4	>3550
Metallic	Hg	68 (16)	0.7	−39
	Al	324 (77)	3.4	660
	Fe	406 (97)	4.2	1538
	W	849 (203)	8.8	3410
van der Waals	Ar	7.7 (1.8)	0.08	−189
	Cl_2	31 (7.4)	0.32	−101
Hydrogen	NH_3	35 (8.4)	0.36	−78
	H_2O	51 (12.2)	0.52	0

Primary bonds

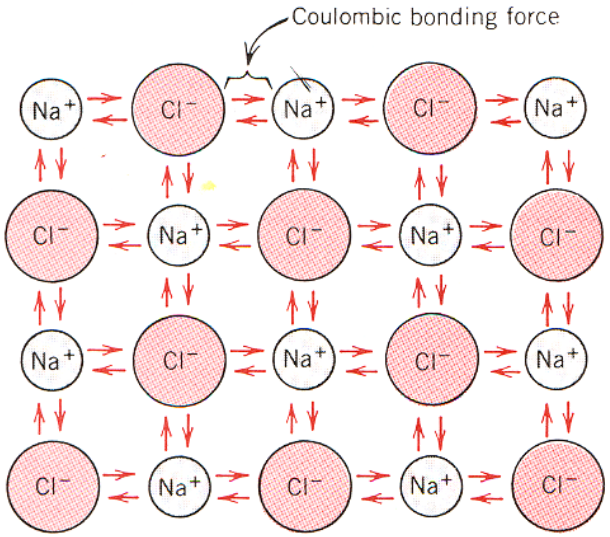

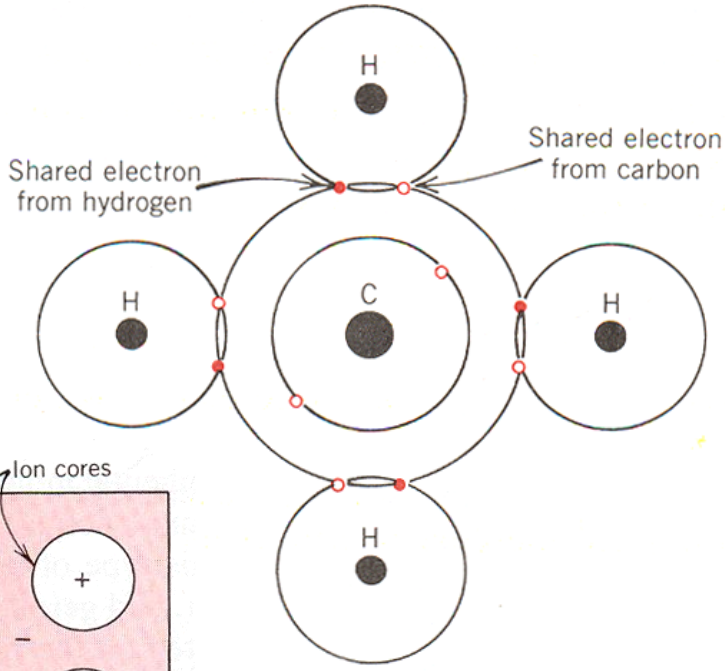

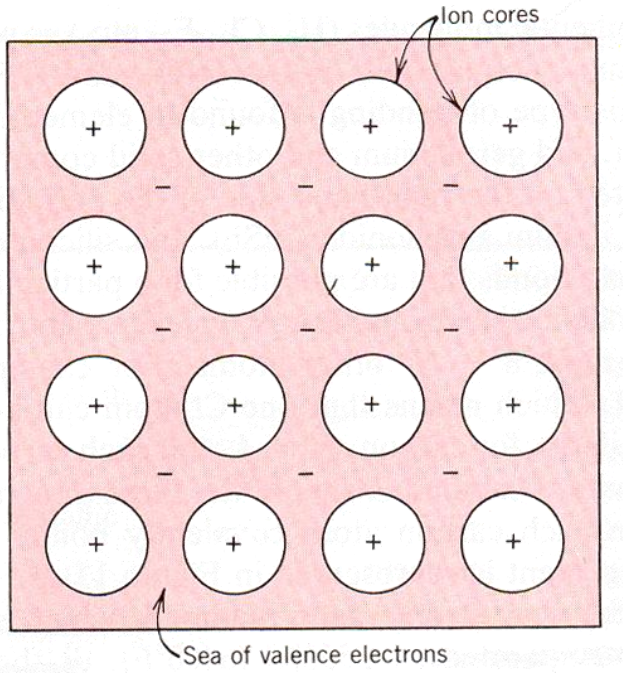

Secondary bonds

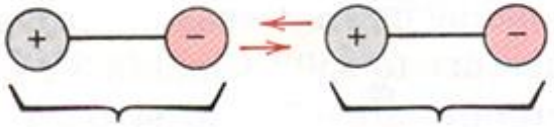

Atomic or molecular dipoles

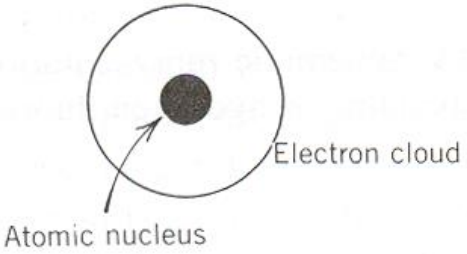

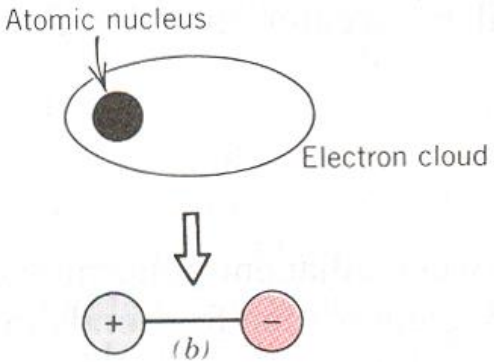

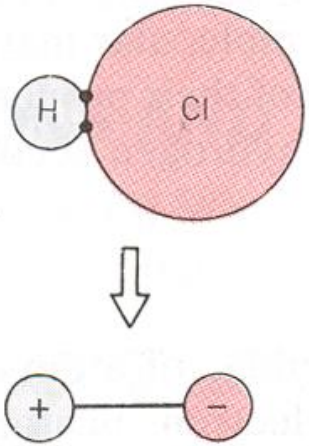

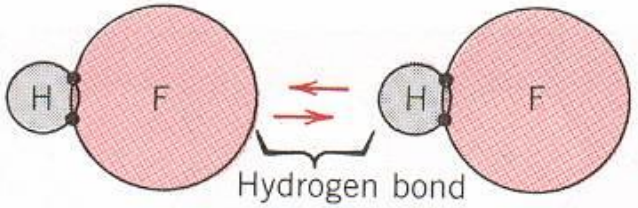

Potential Energy Curves

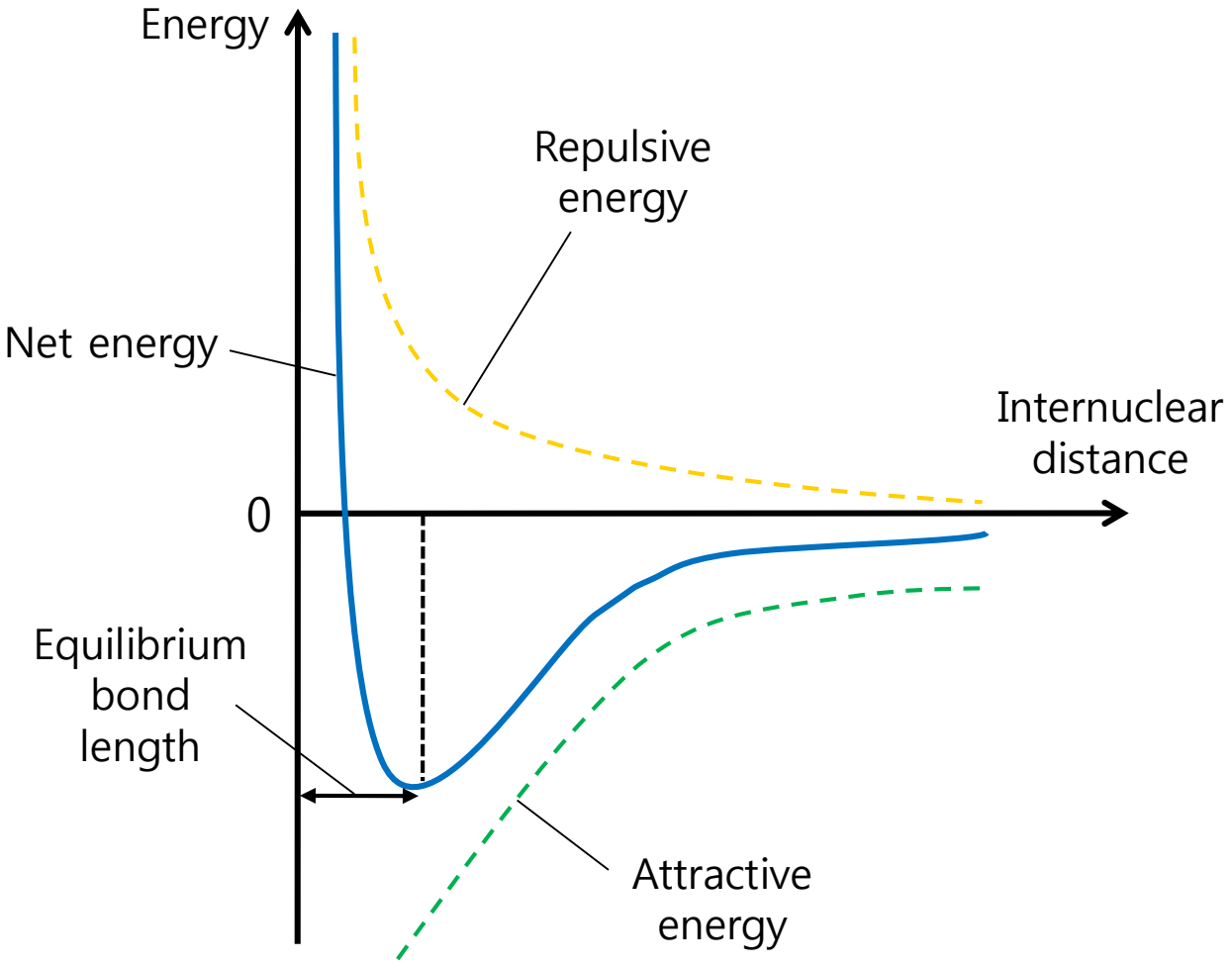

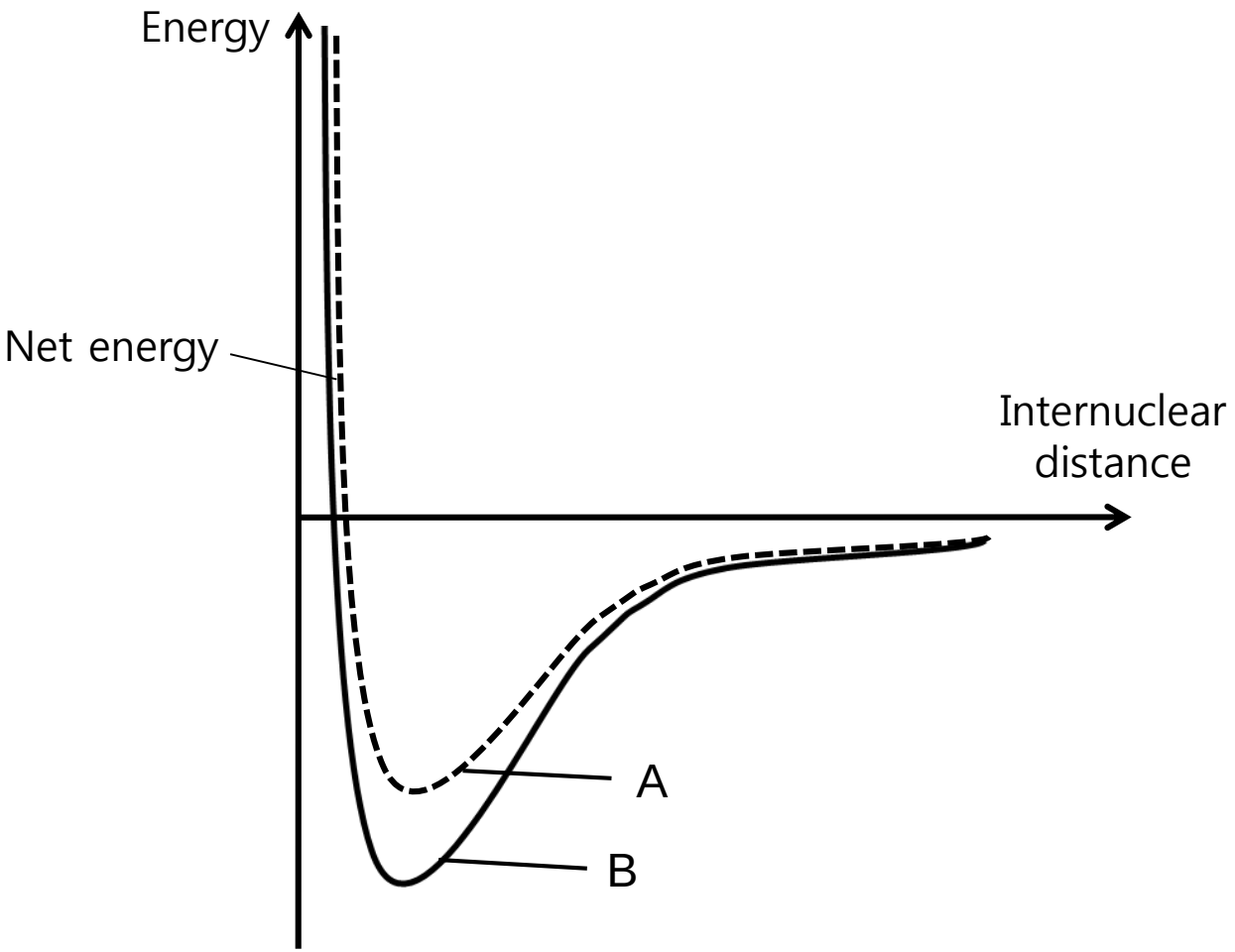

Crystal Structure of Metals

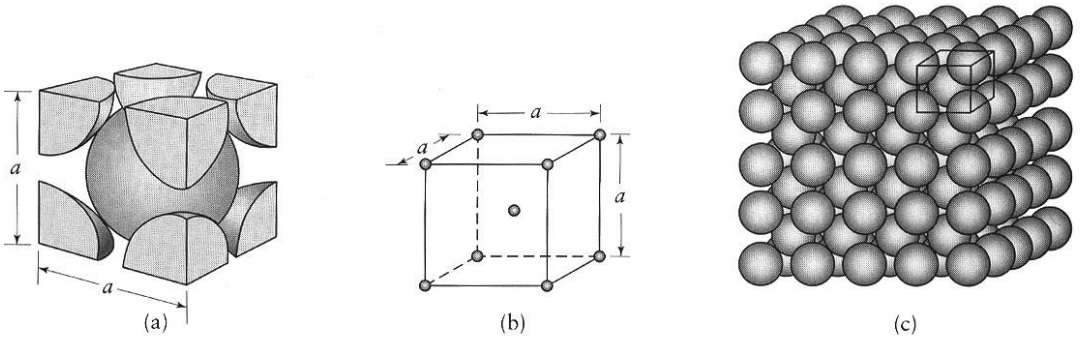

FIGURE 3.2a The body-centered cubic (bcc) crystal structure: (a) hard-ball model; (b) unit cell; and (c) single crystal with many unit cells. *Source*: Courtesy of Dr. William G. Moffatt.

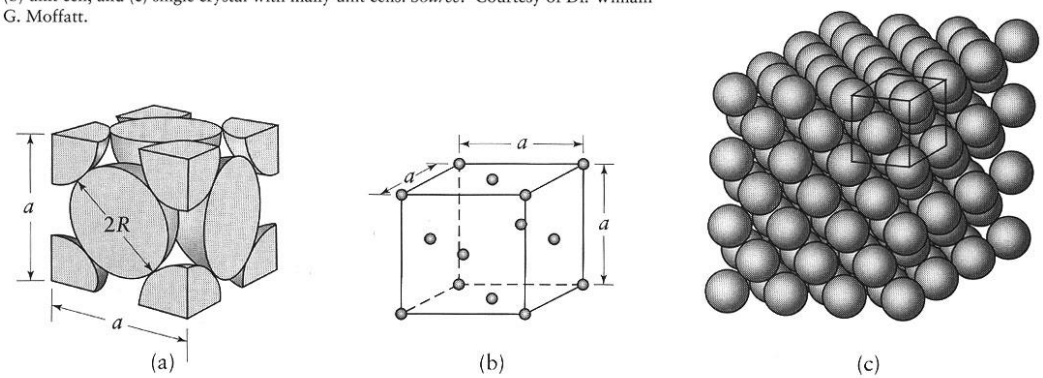

FIGURE 3.2b The face-centered cubic (fcc) crystal structure: (a) hard-ball model; (b) unit cell; and (c) single crystal with many unit cells. *Source*: Courtesy of Dr. William G. Moffatt.

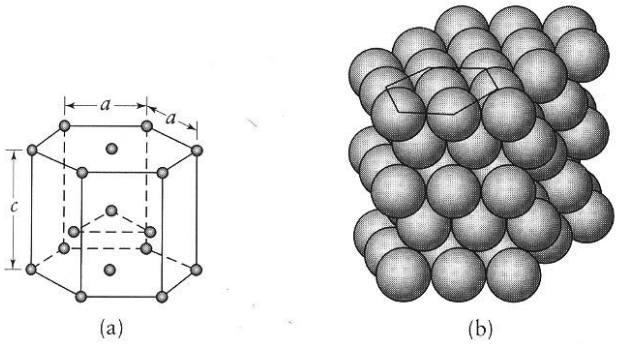

FIGURE 3.2c The hexagonal close-packed (hcp) crystal structure: (a) unit cell; and (b) single crystal with many unit cells. *Source*: Courtesy of Dr. William G. Moffatt.

Crystal – crystalline structure lattice

- 3 basic patterns of atomic arrangement in most metals
- BCC (body-centered cubic)
- FCC (face-centered cubic)
- HCP (hexagonal close-packed)

Crystal Structure of Metals (cont.)

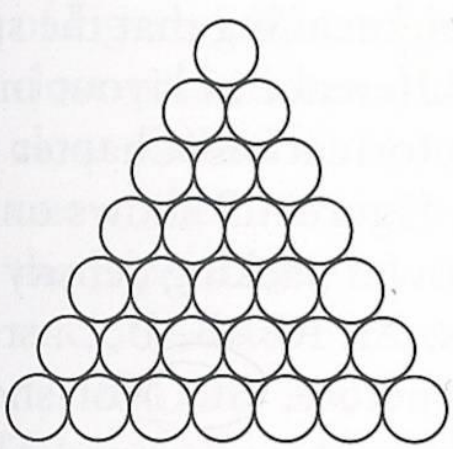

(a) Close-packed layer A

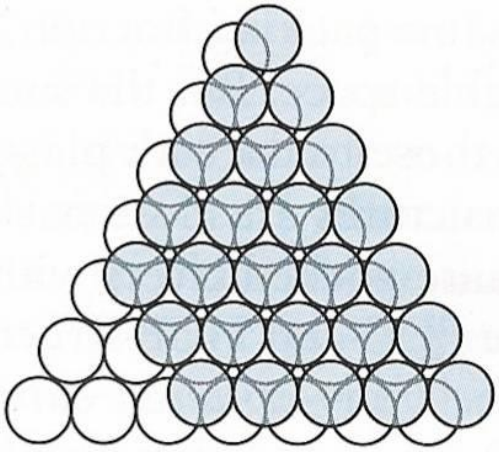

(b) Layer B on layer A to give ABABAB ... or CPH packing

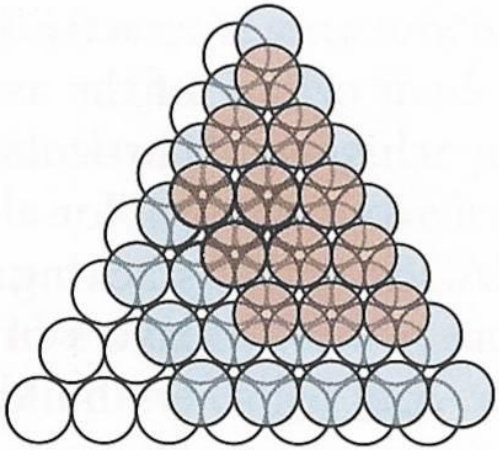

(c) Layer C on layers A and B to give ABCABC ... or FCC packing

(a) A close-packed layer of spheres, layer A; atoms often behave as if hard and spherical. (b) A second layer, B, nesting in the first; repeating this sequence gives ABAB . . . or CPH stacking. (c) A third layer, C, can be nested so that it does not lie above A or B; if repeated this gives ABCABC . . . or FCC stacking.

Crystal Structure of Metals (cont.)

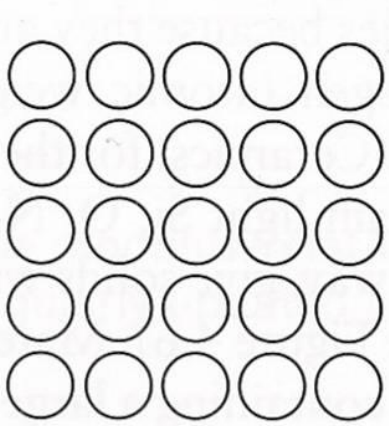

(a) Non-close-packed layer A

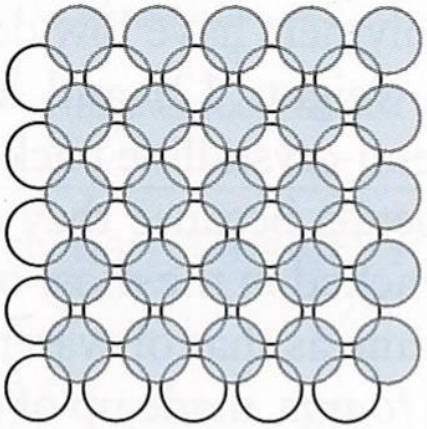

(b) Layer B on layer A to give ABABAB... or BCC packing

(a) A square grid of spheres; it is a less efficient packing than that of the previous figure. (b) A second layer, B, nesting in the first, A; repeating this sequence gives ABAB . . . packing. If the sphere spacing is adjusted so that the gray spheres lie on the corners of a cube, the result is the non-close-packed BCC structure.

Crystal Structure of Metals (cont.)

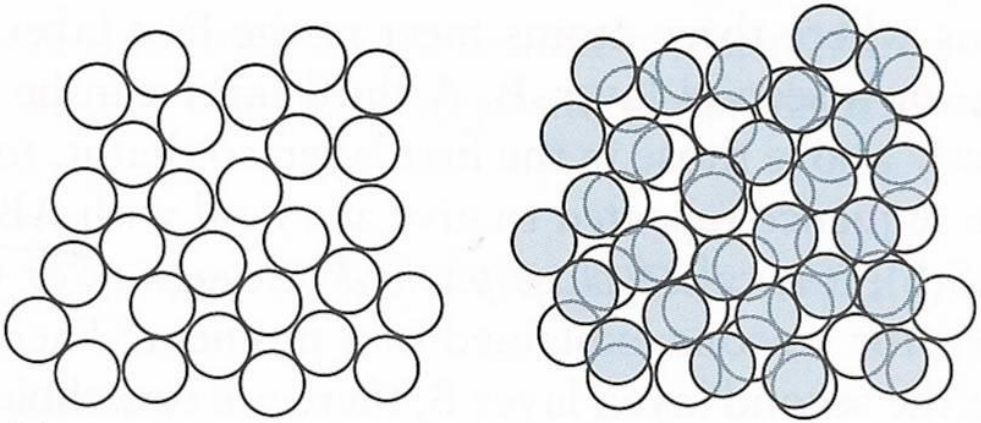

(a) An irregular arrangement of spheres. (b) Extending this in three dimensions gives a random or amorphous structure.

Atomic Packing Factor

Body-centered cubic

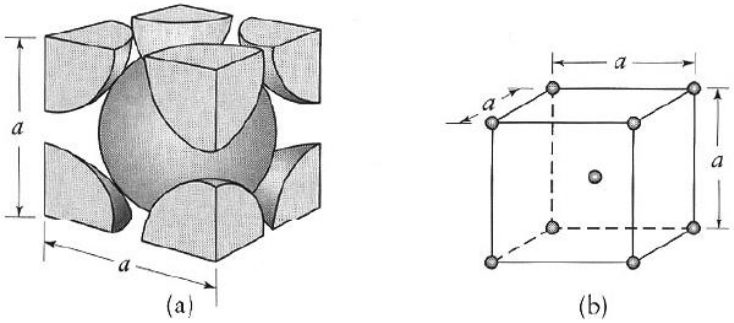

$$\text{Atomic Packing Factor} = \frac{\text{Volume of total spheres}}{\text{Volume of unit cell}}$$

$$\text{For BCC,} \quad \text{APF} = \frac{2 \times \frac{4}{3}\pi(\sqrt{3}a/4)^3}{a^3} = 0.68$$

Face-centered cubic

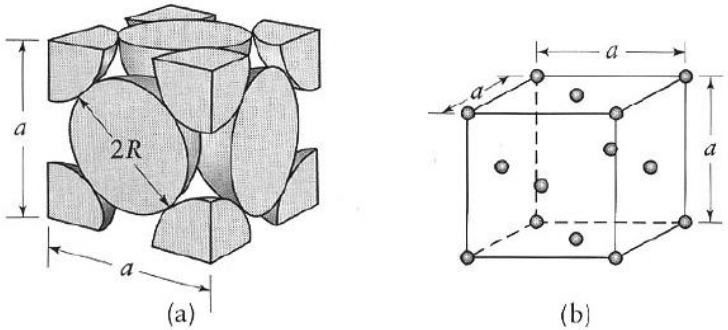

$$\text{For FCC,} \quad \text{APF} = \frac{4 \times \frac{4}{3}\pi(\sqrt{2}a/4)^3}{a^3} = 0.74$$

Hexagonal close-packed

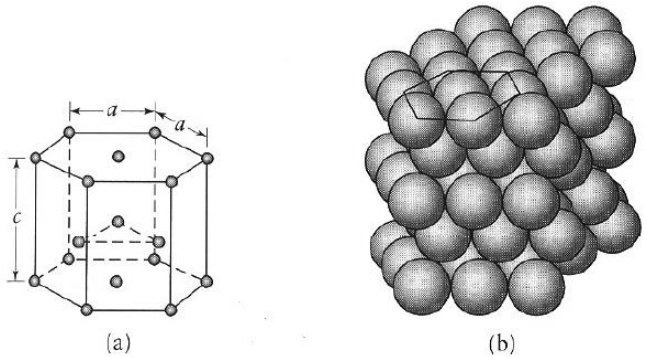

$$\text{For HCP,} \quad \text{APF} = \frac{2 \times \frac{4}{3}\pi(a/2)^3}{2 \times \frac{1}{2}a^2\sin 60° \cdot c} = \frac{2 \times \frac{4}{3}\pi(a/2)^3}{2 \times \frac{1}{2}a^2\sin 60° \cdot \sqrt{\frac{8}{3}}a}$$

$$= 0.74$$

Deformation of Crystal

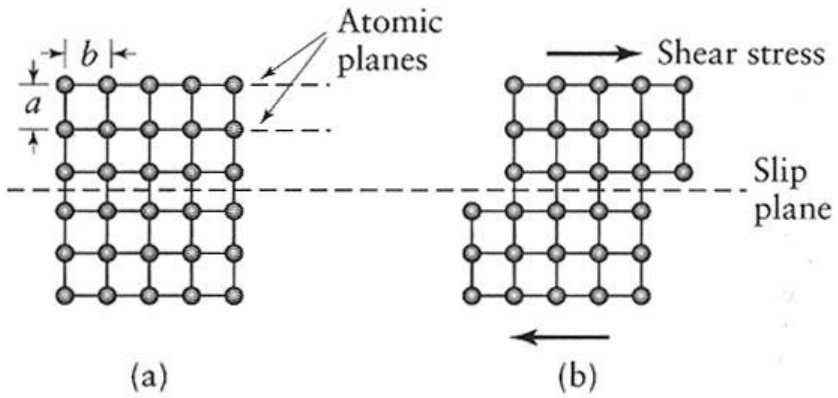

FIGURE 3.3 Permanent deformation, also called plastic deformation, of a single crystal subjected to a shear stress: (a) structure before deformation; and (b) deformation by slip. The b/a ratio influences the magnitude of the shear stress required to cause slip.

elastic deformation

plastic deformation

- slip
- slip band
- twinning

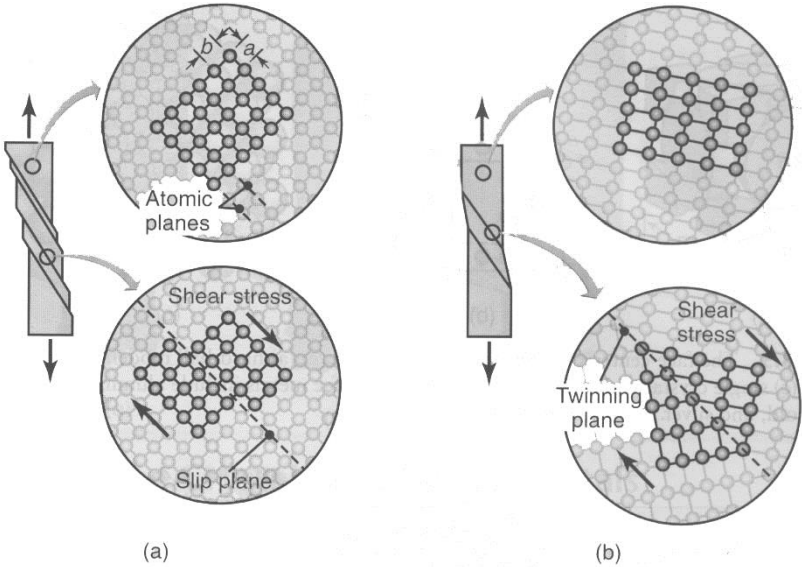

FIGURE 3.5 Permanent deformation of a single crystal under a tensile load. The highlighted grid of atoms emphasizes the motion that occurs within the lattice. (a) Deformation by slip. The b/a ratio influences the magnitude of the shear stress required to cause slip. Note that the slip planes tend to align themselves in the direction of pulling. (b) Deformation by twinning, involving generation of a "twin" around a line of symmetry subjected to shear. Note that the tensile load results in a shear stress in the plane illustrated.

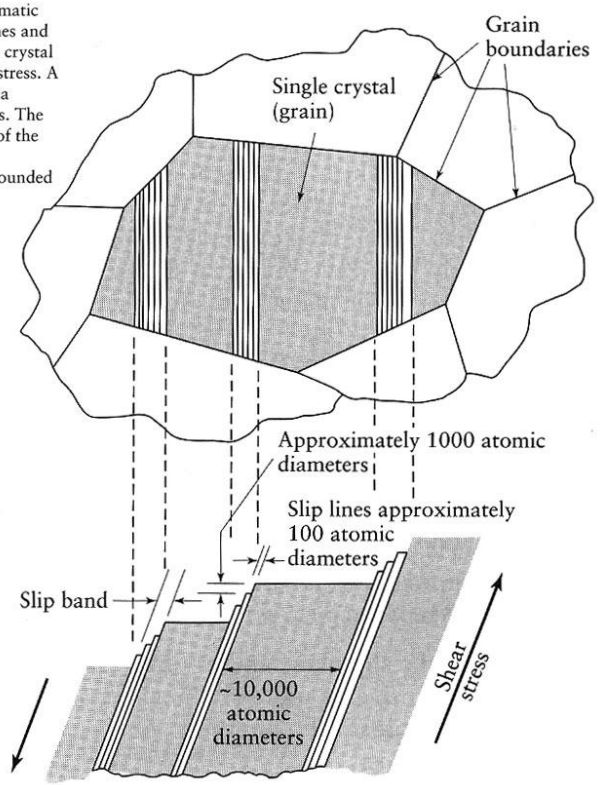

FIGURE 3.6 Schematic illustration of slip lines and slip bands in a single crystal subjected to a shear stress. A slip band consists of a number of slip planes. The crystal at the center of the upper drawing is an individual grain surrounded by other grains.

Strength of single crystal

- **Theoretical shear strength**

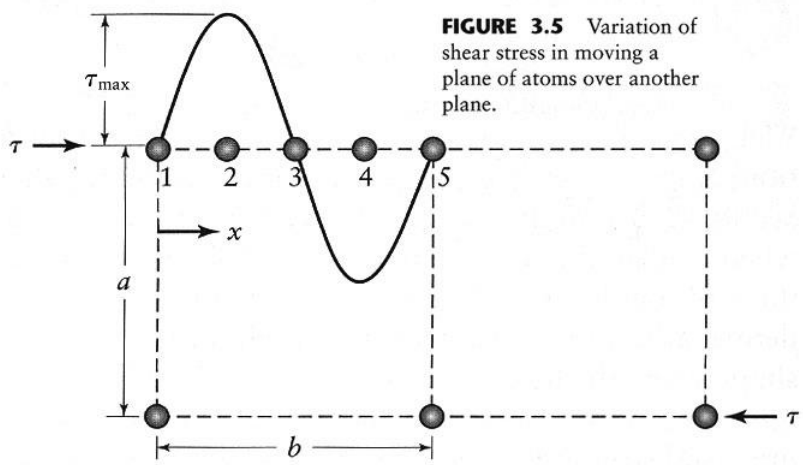

FIGURE 3.5 Variation of shear stress in moving a plane of atoms over another plane.

$$\tau = \tau_{max} \sin\frac{2\pi x}{b} = \tau_{max}\frac{2\pi x}{b} = G\gamma = G\left(\frac{x}{a}\right)$$

$$\tau_{max} = \frac{G}{2\pi}\frac{b}{a}$$

$$\tau_{max} = \frac{G}{2\pi}$$

- **Theoretical tensile strength**

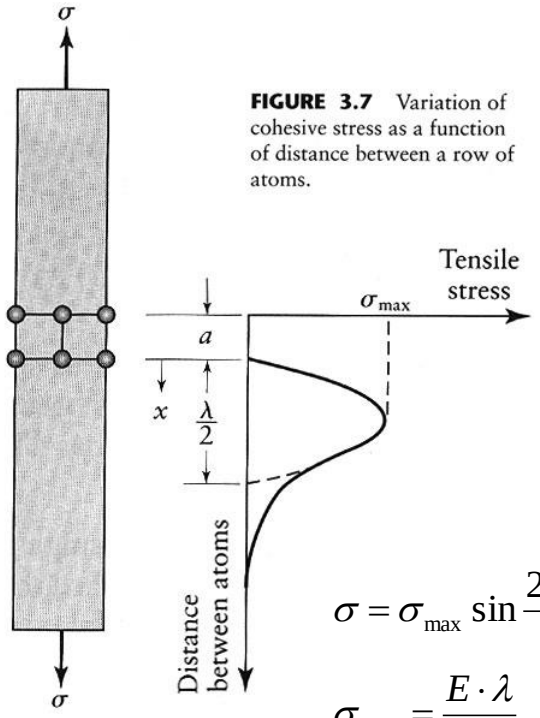

FIGURE 3.7 Variation of cohesive stress as a function of distance between a row of atoms.

$$\sigma = \sigma_{max} \sin\frac{2\pi x}{\lambda} = \sigma_{max}\frac{2\pi x}{\lambda} = \frac{E\cdot x}{a}$$

$$\sigma_{max} = \frac{E\cdot\lambda}{2\pi a}$$

$$\text{Work} = \int_0^{\lambda/2}\sigma_{max}\sin\frac{2\pi x}{\lambda}dx = \frac{\sigma_{max}\cdot\lambda}{\pi}$$

$$\text{Surface energy} = 2\gamma$$

$$\sigma_{max} = \sqrt{\frac{E\gamma}{a}} \cong \frac{E}{10}$$

Strength of single crystal (cont.)

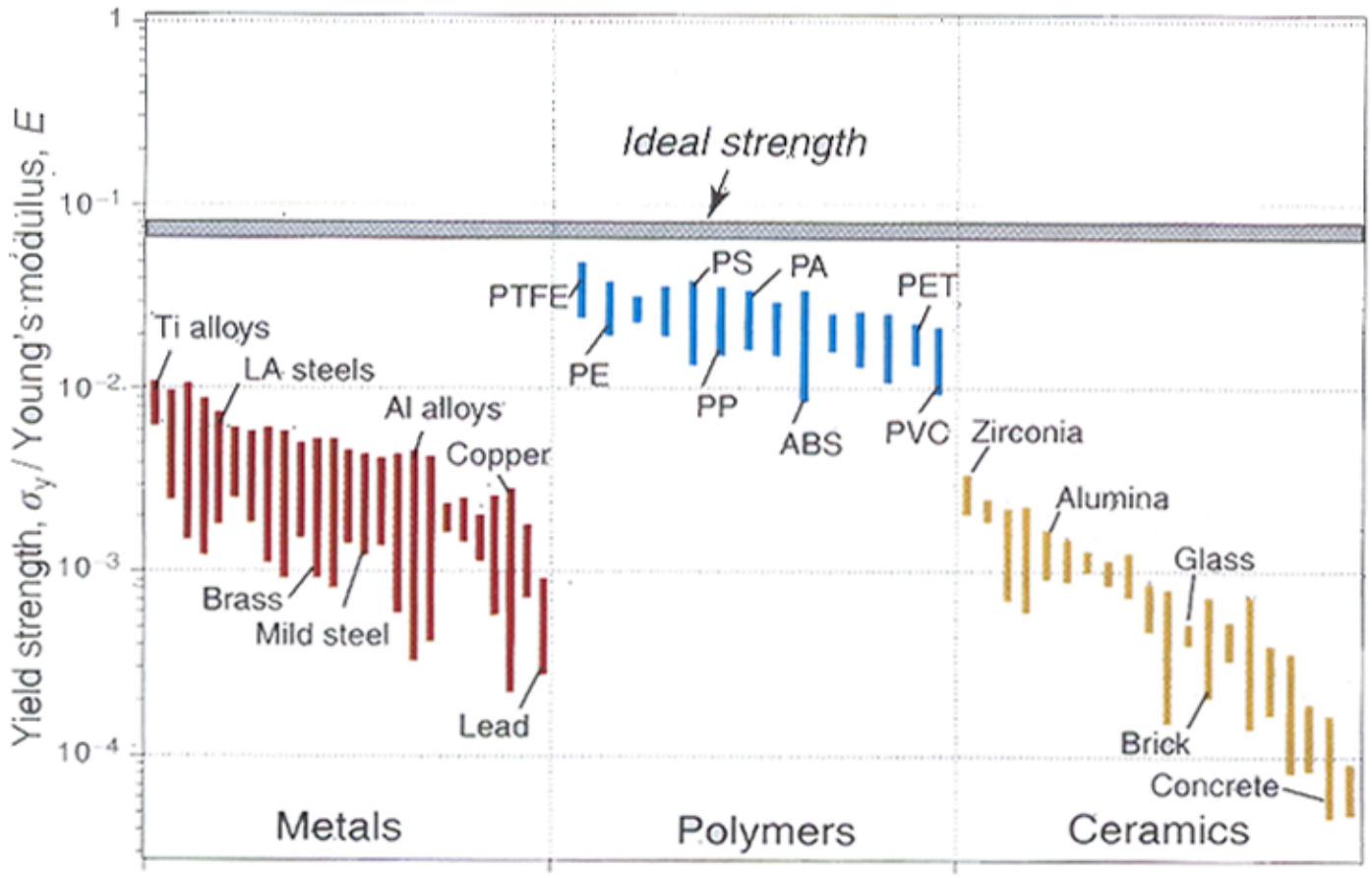

The ideal strength is predicted to be about $E/15$, where E is Young's modulus. The figure shows σ_y/E with a shaded band at the ideal strength.

Imperfections

- **Point defects**
  - Vacancy
  - Interstitial atom
  - Impurity atom
- **Linear defects**
  - Dislocations
- **Planar imperfections**
  - Grain boundary
  - Phase boundary
- **Volume (bulk) imperfections**
  - Voids
  - Inclusions
  - Phases
  - Cracks

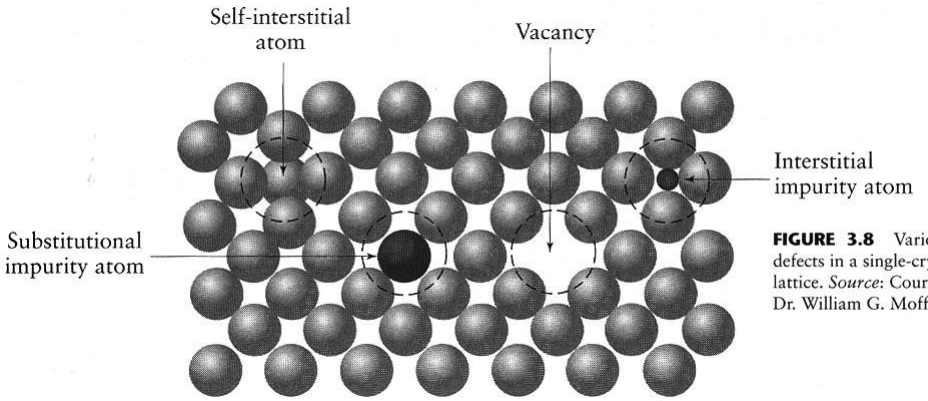

FIGURE 3.8 Various defects in a single-crystal lattice. *Source*: Courtesy of Dr. William G. Moffatt.

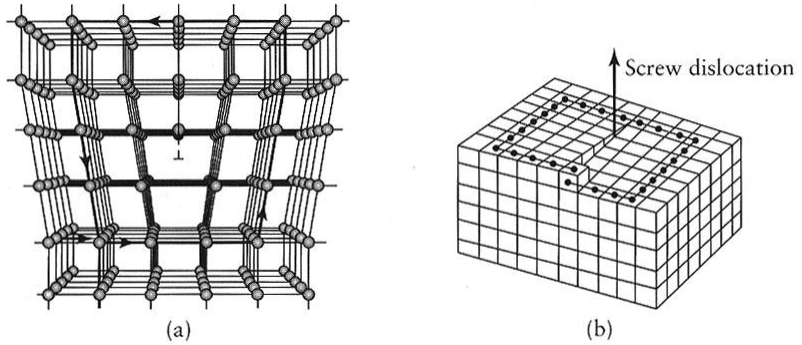

FIGURE 3.9 (a) Edge dislocation, a linear defect at the edge of an extra plane of atoms. (b) Screw dislocation, a helical defect in a three–dimentional lattice of atoms.

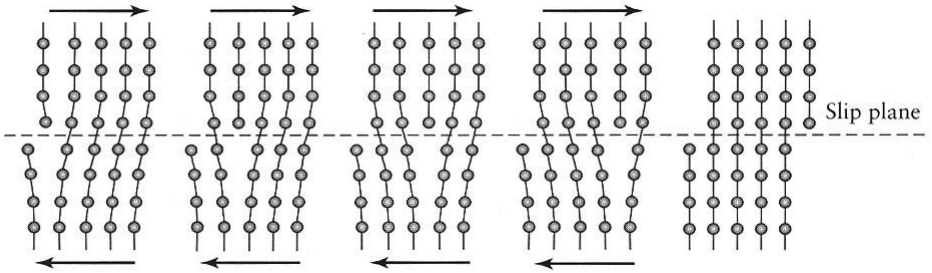

FIGURE 3.10 Movement of an edge dislocation across the crystal lattice under a shear stress. Dislocations help explain why the actual strength of metals is much lower than that predicted by theory.

Imperfections (cont.)

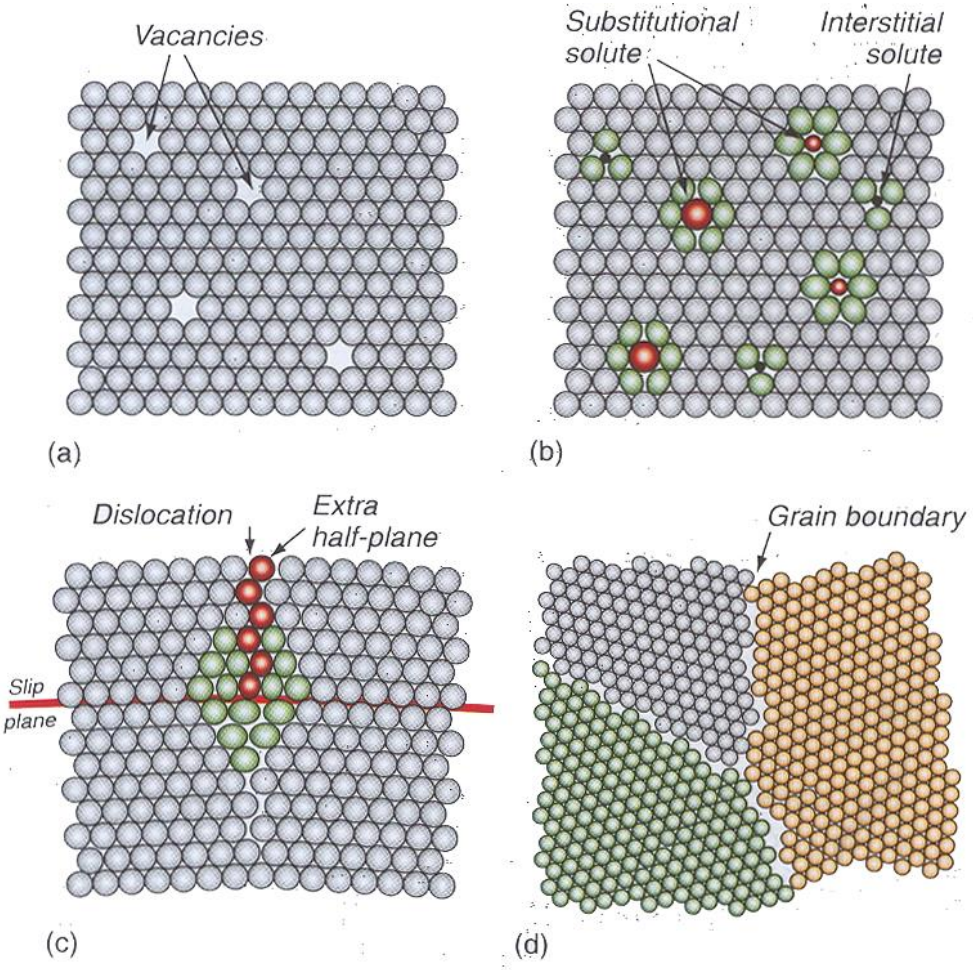

Defects in crystals. (a) Vacancies–missing atoms. (b) Foreign (solute) atom on interstitial and substitutional sites. (c) A dislocation–an extra half-plane of atoms. (d) Grain boundaries.

Grains & Grain boundaries

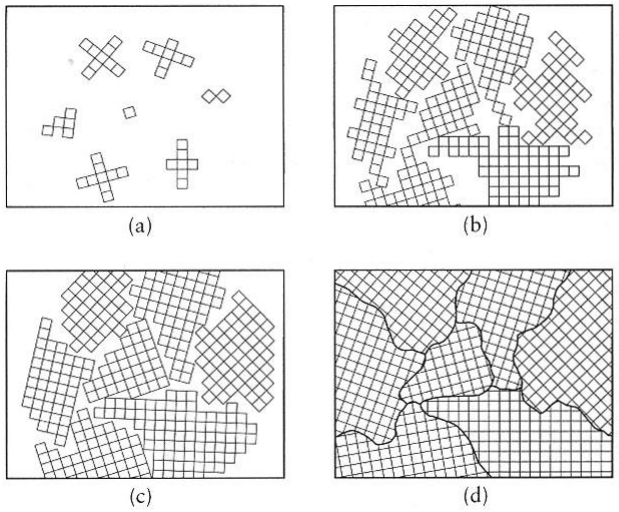

FIGURE 3.11 Schematic illustration of the various stages during solidification of molten metal. Each small square represents a unit cell. (a) Nucleation of crystals at random sites in the molten metal. Note that the crystallographic orientation of each site is different. (b) and (c) Growth of crystals as solidification continues. (d) Solidified metal, showing individual grains and grain boundaries. Note the different angles at which neighboring grains meet each other. *Source*: W. Rosenhain.

FIGURE 3.12 Variation of tensile stress across a plane of polycrystalline metal specimen subjected to tension. Note that the strength exhibited by each grain depends on its orientation.

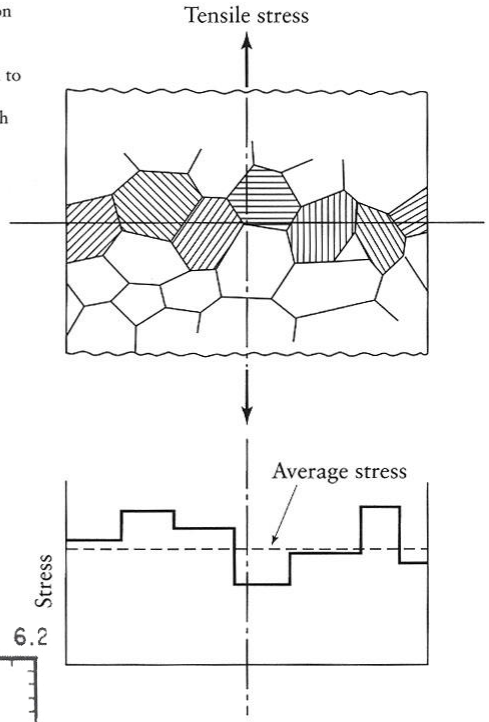

- **Hall-Petch equation**

$$Y = Y_i + kd^{-\frac{1}{2}}$$

$$N = 2^{n-1}$$

- **ASTM : American Society for Testing and Materials**

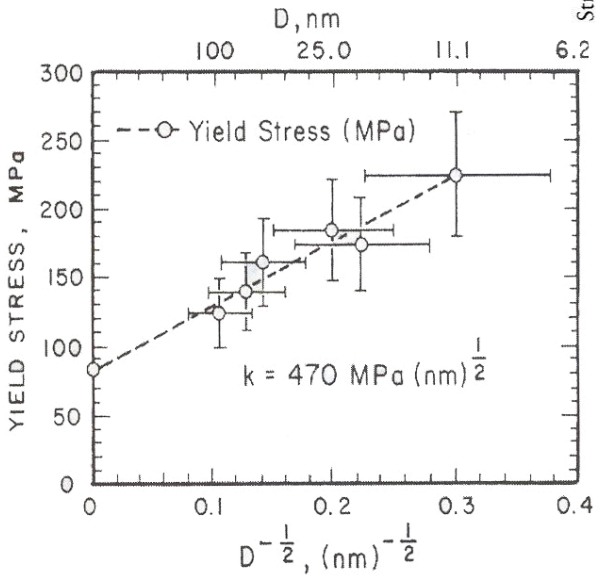

그림 1-11 Cu 나노 결정 재료의 홀 · 펫취의 관계식

Plastic Deformation-Polycrystalline Metal

- **Anisotropy (이방성)**

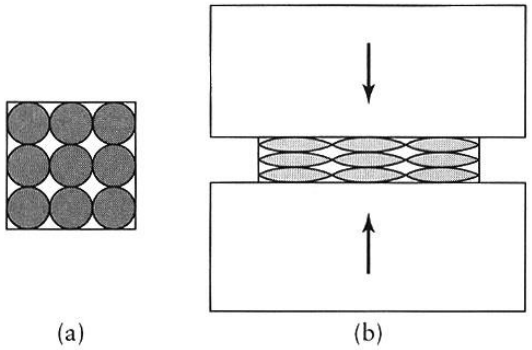

FIGURE 3.14 Plastic deformation of idealized (equiaxed) grains in a specimen subjected to compression, such as is done in rolling or forging of metals: (a) before deformation; and (b) after deformation. Note the alignment of grain boundaries along a horizontal direction.

- **Preferred orientation (선택적 방향성)**
  - Tension-slip directions align with the loading direction
  - Compression-slip perpendicular to the loading direction

- **Mechanical fibering**
  - Alignment of impurities, inclusions, and voids
  - Weaken grain boundaries-week/less ductile in vertical direction

Recovery, Recrystallization and Grain growth

FIGURE 3.16 Schematic illustration of the effects of recovery, recrystallization, and grain growth on mechanical properties and shape and size of grains. Note the formation of small new grains during recrystallization. *Source*: G. Sachs.

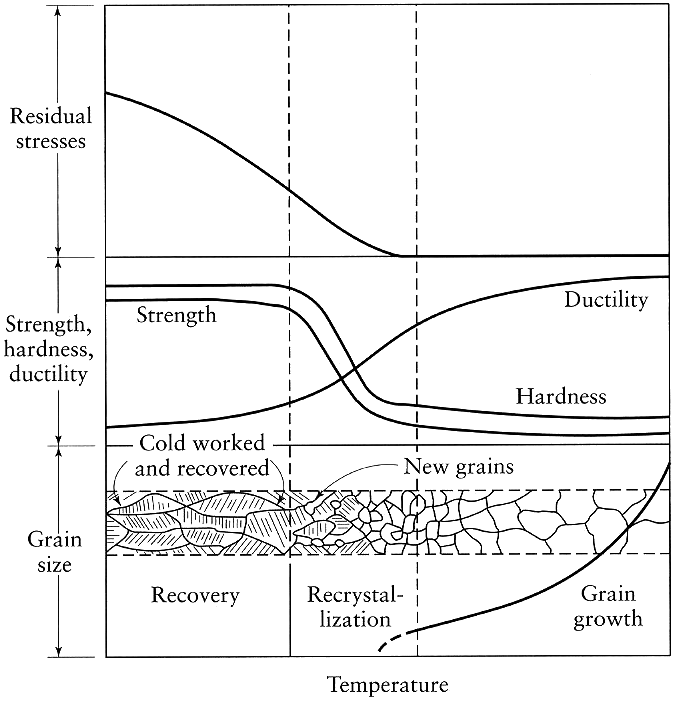

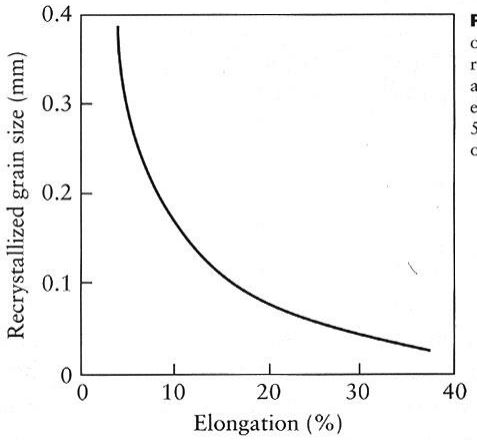

FIGURE 3.18 The effect of prior cold work on the recrystallized grain size of alpha brass. Below a critical elongation (strain), typically 5%, no recrystallization occurs.

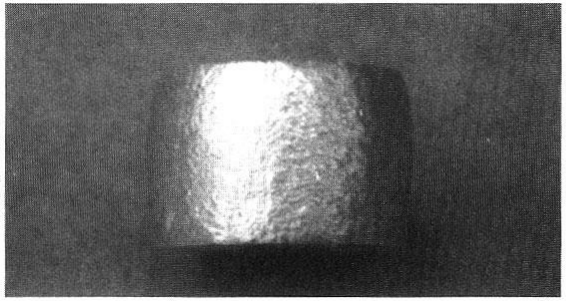

FIGURE 3.19 Surface roughness on the cylindrical surface of an aluminum specimen subjected to compression. *Source*: A. Mulc and S. Kalpakjian.

TABLE 3.1

Homologous Temperature Ranges for Various Processes

Process	T/T_m
Cold working	<0.3
Warm working	0.3 to 0.5
Hot working	>0.6

Failure (파손) and Fracture (파괴)

- **Buckling**
  - Out-of plane deformation

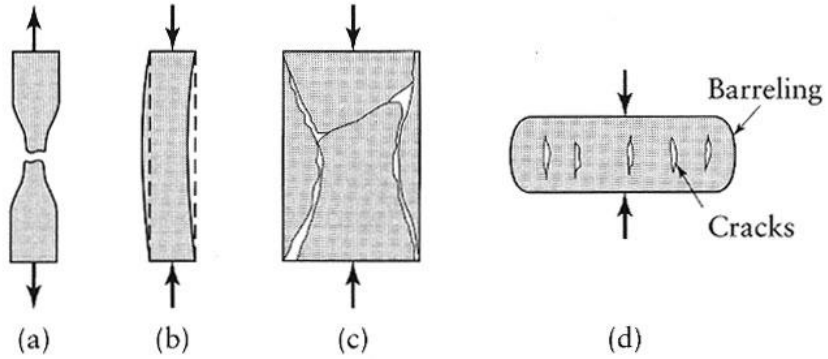

FIGURE 3.20 Schematic illustration of types of failure in materials: (a) necking and fracture of ductile materials; (b) buckling of ductile materials under a compressive load; (c) fracture of brittle materials in compression; (d) cracking on the barreled surface of ductile materials in compression. (See also Fig. 6.1b)

- **Fracture**
  - Ductile fracture
    - Shear
  - Brittle fracture
    - Tensile

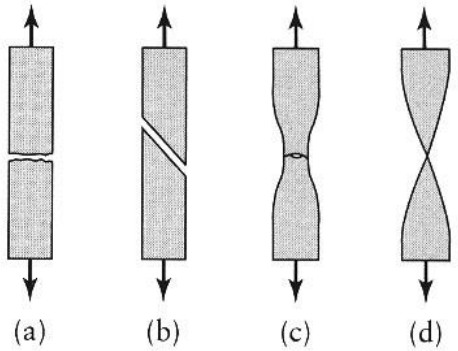

FIGURE 3.21 Schematic illustration of the types of fracture in tension: (a) brittle fracture in polycrystalline metals; (b) shear fracture in ductile single crystals (see also Fig. 3.4a); (c) ductile cup-and-cone fracture in polycrystalline metals (see also Fig. 2.2); (d) complete ductile fracture in polycrystalline metals, with 100% reduction of area.

Ductile Fracture

- **Fibrous pattern with dimples**

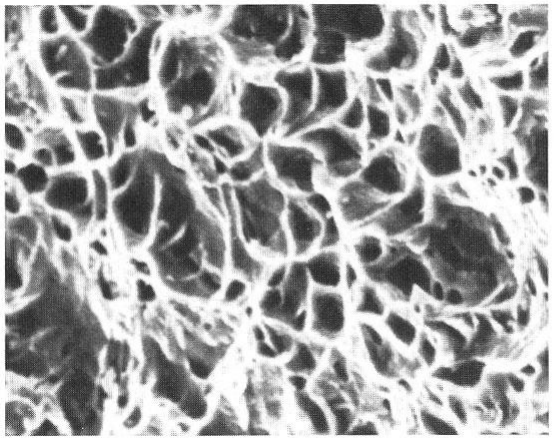

FIGURE 3.22 Surface of ductile fracture in low-carbon steel, showing dimples. Fracture is usually initiated at impurities, inclusions, or preexisting voids in the metal. *Source*: K.-H. Habig and D. Klaffke. Photo by BAM, Berlin, Germany.

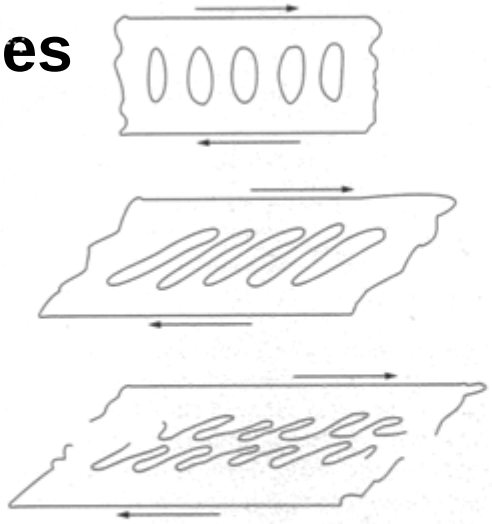

FIGURE 3.23 A schematic illustration of the mechanism of ductile fracture. Note the formation of elongated dimples on the fracture surface. *Source:* After H. C. Rogers.

and propagates to the periphery of this necked region. Because of its appearance, the fracture surface of a tension-test specimen is call a **cup-and-cone fracture** (Fig. 3.21c).

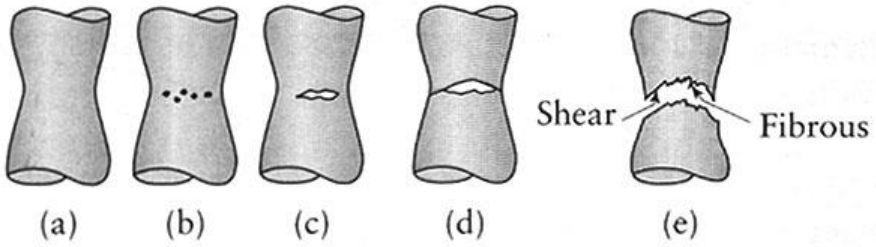

FIGURE 3.23 Sequence of events in necking and fracture of a tensile-test specimen: (a) early stage of necking; (b) small voids begin to form within the necked region; (c) voids coalesce, producing an internal crack; (d) rest of cross-section begins to fail at the periphery by shearing; (e) final fracture surfaces, known as cup-(top fracture surface) and-cone (bottom surface) fracture.

Ductile Fracture (2)

- **Effect of inclusions**
- **Transition temp.**
- **Strain aging**

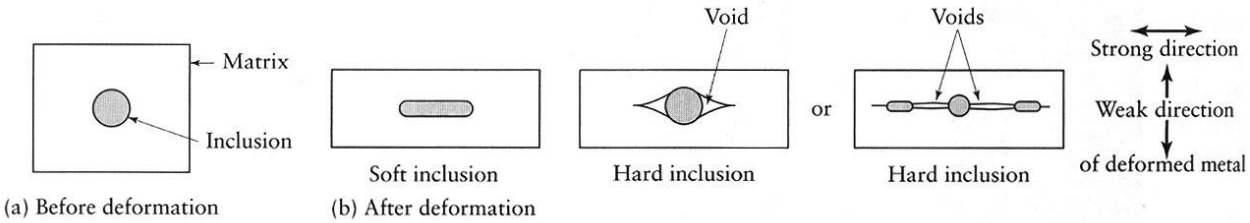

FIGURE 3.25 Schematic illustration of the deformation of soft and hard inclusions and their effect on void formation in plastic deformation. Note that hard inclusions, because they do not comply with the overall deformation of the ductile matrix, can cause voids.

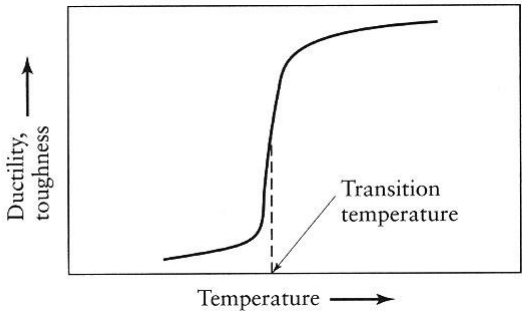

FIGURE 3.26 Schematic illustration of transition temperature. Note the narrow temperature range across which the behavior of the metal undergoes a major transition.

FIGURE 3.24 The effect of volume fraction of various second-phase particles on the true strain at fracture in a tensile test for copper. *Source*: After B. I. Edelson and W. M. Baldwin.

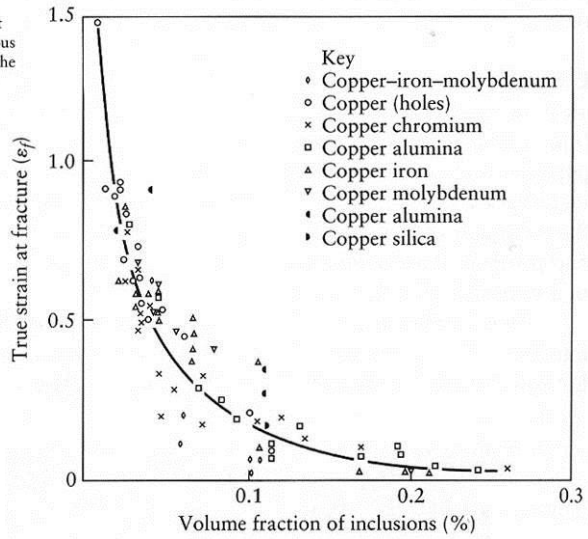

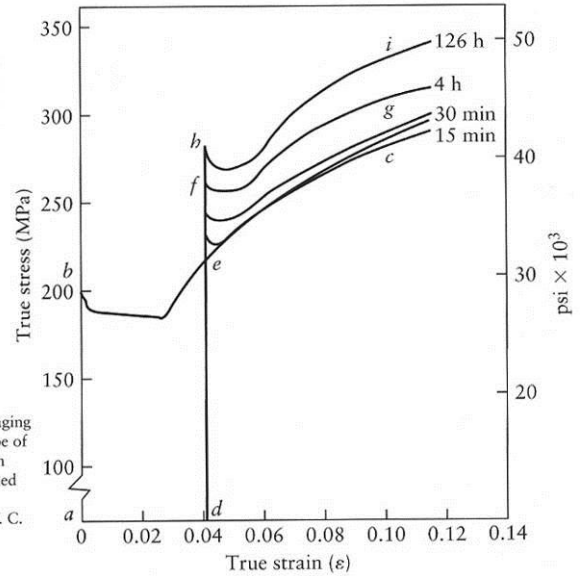

FIGURE 3.27 Strain aging and its effect on the shape of the true-stress–true-strain curve for 0.03% C rimmed steel at 60°C (140°F). *Source*: A. S. Keh and W. C. Leslie.

Brittle Facture

- **Cleavage plane – max. tensile stress**

FIGURE 3.28 Typical fracture surface of steel that has failed in a brittle manner. The fracture path is transgranular (through the grains). Compare this surface with the ductile fracture surface shown in Fig. 3.22. Magnification: 200×. *Source*: Courtesy of Packer Engineering.

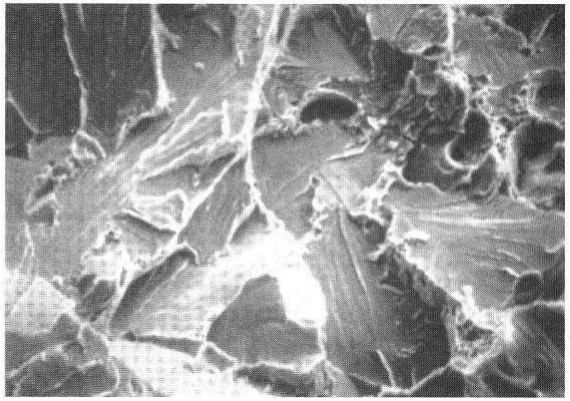

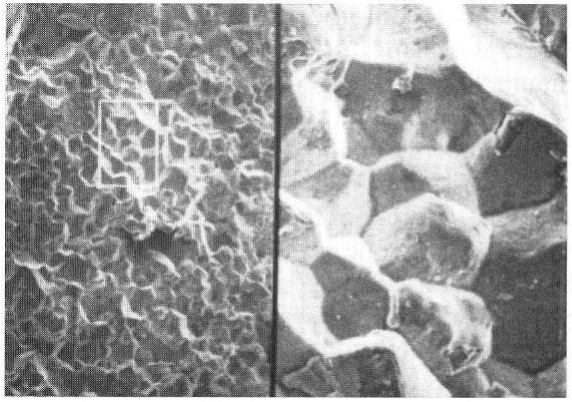

FIGURE 3.29 Intergranular fracture, at two different magnifications. Grains and grain boundaries are clearly visible in this micrograph. The fracture path is along the grain boundaries. Magnification: left, 100×; right, 500×. *Source*: Courtesy of Packer Engineering.

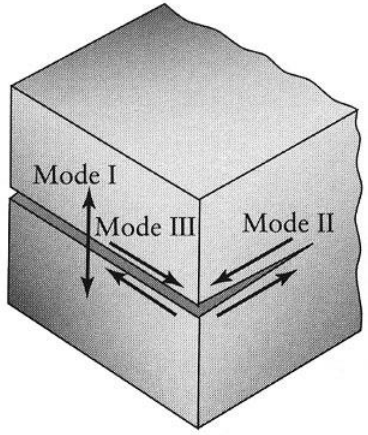

FIGURE 3.30 Three modes of fracture. Mode I has been studied extensively, because it is the most commonly observed in engineering structures and components. Mode II is rare. Mode III is the tearing process; examples include opening a pop-top can, tearing a piece of paper, and cutting materials with a pair of scissors.

Brittle Facture (2)

- **Fatigue fracture**
  - beach marks, striations

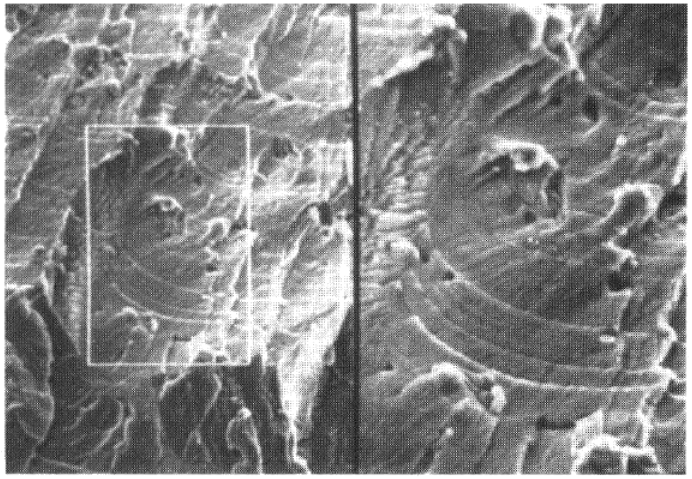

FIGURE 3.31 Typical fatigue fracture surface on metals, showing beach marks. Most components in machines and engines fail by fatigue and not by excessive static loading. Magnification: left, 500×; right, 1000×. *Source*: Courtesy of Packer Engineering.

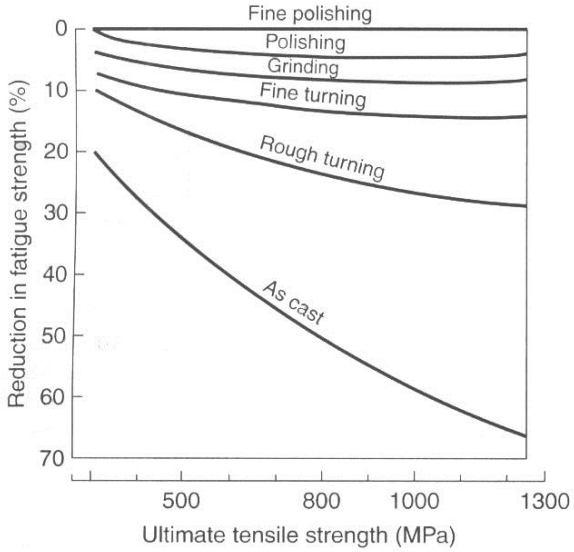

(a)

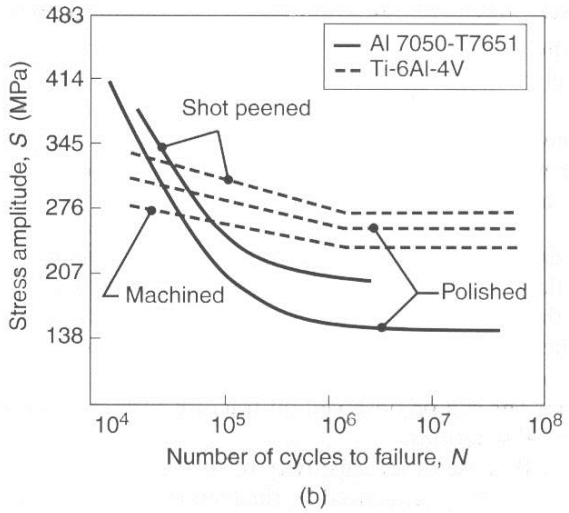

(b)

FIGURE 3.32 Reduction in fatigue strength of cast steels subjected to various surface-finishing operations. (a) Effect of surface roughness. Note that the reduction is greater as the surface roughness and strength of the steel increase. *Source:* After J.E. Shigley and L.D. Mitchell. (b) Effect of residual stress, as developed by shot peening (see Section 4.5.1). *Source:* After B.J. Hamrock, S.R. Schmid, and B.O. Jacobson.

Size Effect

- **Smaller, stronger**
- **Whisker**
- **CNT**

SiC whisker
(0.5 micro meter dia.)

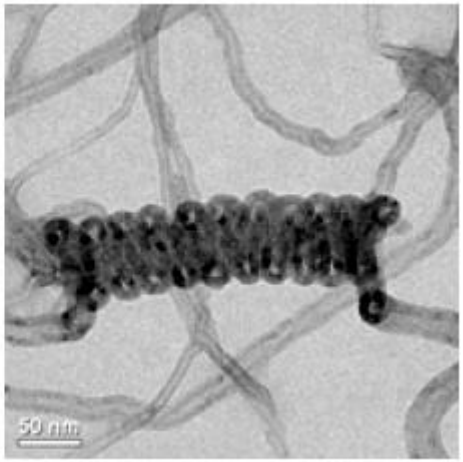

Multiwall CNT
(20 nano meter dia.)

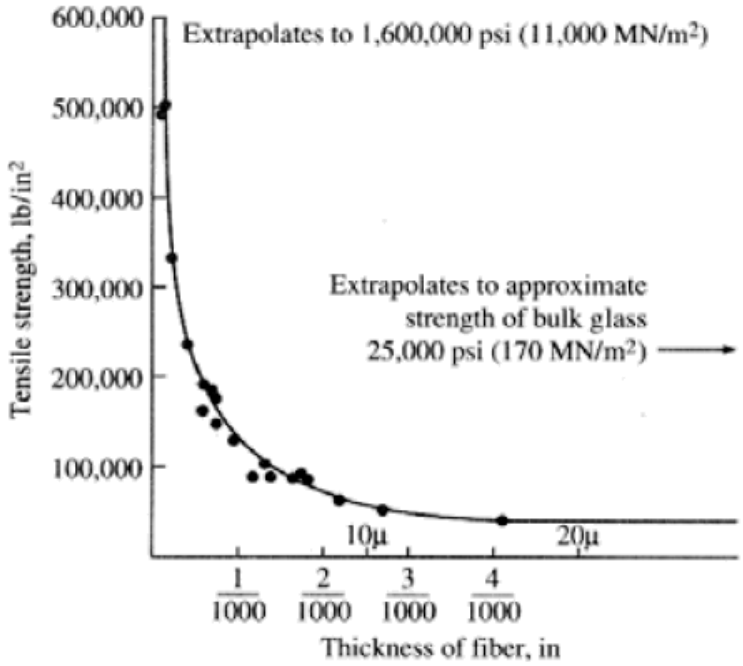

Physical Properties

TABLE 3.2
Physical Properties of Various Materials at Room Temperature

	Density (kg/m^3)	Melting Point (°C)	Specific Heat (J/kg K)	Thermal Conductivity (W/m K)	Coefficient of Thermal Expansion ($\mu m/m°C$)
METAL					
Aluminum	2700	660	900	222	23.6
Aluminum alloys	2630–2820	476–654	880–920	121–239	23.0–23.6
Beryllium	1854	1278	1884	146	8.5
Columbium (niobium)	8580	2468	272	52	7.1
Copper	8970	1082	385	393	16.5
Copper alloys	7470–8940	885–1260	337–435	29–234	16.5–20
Gold	19300	1063	129	317	19.3
Iron	7860	1537	460	74	11.5
Steels	6920–9130	1371–1532	448–502	15–52	11.7–17.3
Lead	11350	327	130	35	29.4
Lead alloys	8850–11,350	182–326	126–188	24–46	27.1–31.1
Magnesium	1745	650	1025	154	26.0
Magnesium alloys	1770–1780	610–621	1046	75–138	26.0
Molybdenum alloys	10210	2610	276	142	5.1
Nickel	8910	1453	440	92	13.3
Nickel alloys	7750–8850	1110–1454	381–544	12–63	12.7–18.4
Silicon	2330	1423	712	148	7.63
Silver	10500	961	235	429	19.3
Tantalum alloys	16600	2996	142	54	6.5
Titanium	4510	1668	519	17	8.35
Titanium alloys	4430–4700	1549–1649	502–544	8–12	8.1–9.5
Tungsten	19290	3410	138	166	4.5
NONMETALLIC					
Ceramics	2300–5500	–	750–950	10–17	5.5–13.5
Glasses	2400–2700	580–1540	500–850	0.6–1.7	4.6–70
Graphite	1900–2200	–	840	5–10	7.86
Plastics	900–2000	110–330	1000–2000	0.1–0.4	72–200
Wood	400–700	–	2400–2800	0.1–0.4	2–60

- **Density**
- **Melting point**
- **Specific heat**
- **Thermal conductivity**
- **CTE**

Ferrous Alloys

- **Carbon steel**
  - More carbon, higher hardenability, strength, hardness, wear resistance, lower ductility, weldability, toughness
  - Low-carbon steel (<0.3%)
  - Medium-carbon steel (0.3~0.6%)
  - High-carbon steel (>0.6%)

- **Alloy steel**

Ferrous Alloys (2)

- **Stainless steel**
  - Chromium oxide film

TABLE 3.3

Room-Temperature Mechanical Properties and Typical Applications of Annealed Stainless Steels

AISI (UNS)	Ultimate Tensile Strength (MPa)	Yield Strength (MPa)	Elongation (%)	Characteristics and Typical Applications
303 (S30300)	550–620	240–260	50–53	Screw-machine products, shafts, valves, bolts, bushings, and nuts; aircraft fittings; rivets; screws; studs.
304 (S30400)	565–620	240–290	55–60	Chemical and food-processing equipment, brewing equipment, cryogenic vessels, gutters, downspouts, and flashings.
316 (S31600)	550–590	210–290	55–60	High corrosion resistance and high creep strength. Chemical and pulp-handling equipment, photographic equipment, brandy vats, fertilizer parts, ketchup-cooking kettles, and yeast tubs.
410 (S41000)	480–520	240–310	25–35	Machine parts, pump shafts, bolts, bushings, coal chutes, cutlery, fishing tackle, hardware, jet engine parts, mining machinery, rifle barrels, screws, and valves.
416 (S41600)	480–520	275	20–30	Aircraft fittings, bolts, nuts, fire extinguisher inserts, rivets, and screws.

Ferrous Alloys (3)

- **Tool and die steel**
  - High Speed Steel (HSS)

TABLE 3.4

Basic Types of Tool and Die Steels

Type	AISI
High speed	M (molybdenum base)
	T (tungsten base)
Hot work	H1 to H19 (chromium base)
	H20 to H39 (tungsten base)
	H40 to H59 (molybdenum base)
Cold work	D (high carbon, high chromium)
	A (medium alloy, air hardening)
	O (oil hardening)
Shock resisting	S
Mold steels	P1 to P19 (low carbon)
	P20 to P39 (others)
Special purpose	L (low alloy)
	F (carbon–tungsten)
Water hardening	W

Aluminum and Aluminum Alloys

- **High strength-to-weight ratio, corrosion resistance, high thermal and electrical conductivity**

TABLE 3.6

Properties of Various Aluminum Alloys at Room Temperature

Alloy (UNS)	Temper	Ultimate Tensile Strength (MPa)	Yield Strength (MPa)	Elongation in 50 mm (%)
1100 (A91100)	O	90	35	35–45
1100	H14	125	120	9–20
2024 (A92024)	O	190	75	20–22
2024	T4	470	325	19–20
3003 (A93003)	O	110	40	30–40
3003	H14	150	145	8–16
5052 (A95052)	O	190	90	25–30
5052	H34	260	215	10–14
6061 (A96061)	O	125	55	25–30
6061	T6	310	275	12–17
7075 (A97075)	O	230	105	16–17
7075	T6	570	500	11

Aluminum and Aluminum Alloys (2)

TABLE 3.7

Manufacturing Properties and Typical Applications of Wrought Aluminum Alloys

	Characteristics*			
Alloy	Corrosion Resistance	Machinability	Weldability	Typical Applications
1100	A	D–C	A	Sheet-metal work, spun hollow parts, tin-stock.
2014	C	C–B	C–B	Heavy-duty forgings, plate and extrusions for aircraft structural components, wheels.
3003	A	D–C	A	Cooking utensils, chemical equipment, pressure vessels, sheet-metal work, builders' hardware, storage tanks.
5054	A	D–C	A	Welded structures, pressure vessels, tube for marine uses.
6061	B	D–C	A	Trucks, canoes, furniture, structural applications.
7005	D	B–D	B	Extruded structural members, large heat exchangers, tennis racquets, softball bats.

* From A (excellent) to D (poor).

Magnesium and Magnesium Alloys

- **Lightest engineering metal, good vibration-damping characteristics**

TABLE 3.8

Properties and Typical Forms of Various Wrought Magnesium Alloys

Alloy	Composition (%) Al	Zn	Mn	Zr	Condition	Ultimate Tensile Strength (MPa)	Yield Strength (MPa)	Elongation in 50 mm (%)	Typical Forms
AZ31B	3.0	1.0	0.2		F	260	200	15	Extrusions
					H24	290	220	15	Sheet and plates
AZ80A	8.5	0.5	0.2		T5	380	380	7	Extrusions and forgings
HK31A*				0.7	H24	255	255	8	Sheet and plates
ZK60A		5.7		0.55	T5	365	365	11	Extrusions and forgings

* HK31A also contains 3%Th.

Copper and Copper Alloys

- **Best conductors of electricity and heat**

TABLE 3.9

Properties and Typical Applications of Various Wrought Copper and Brasses

Type and UNS Number	Nominal Composition (%)	Ultimate Tensile Strength (MPa)	Yield Strength (MPa)	Elongation in 50 mm (%)	Typical Applications
Oxygen-free electronic (C10100)	99.99 Cu	220–450	70–365	55–4	Bus bars, waveguides, hollow conductors, lead in wires, coaxial cables and tubes, microwave tubes, rectifiers.
Red brass, 85% (C23000)	85.0 Cu 15.0 Zn	270–72	70–435	55–3	Weather stripping, conduit, sockets, fasteners, fire extinguishers, condenser and heat-exchanger tubing.
Low Brass, 80% (C24000)	80.0 Cu 20.0 Zn	300–850	80–450	55–3	Battery caps, bellows, musical instruments, clock dials, flexible hose.
Free-cutting brass (C36000)	61.5 Cu, 3.0 Pb, 35.5 Zn	340–470	125–310	53–18	Gears, pinions, automatic high-speed screw-machine parts.
Naval brass (C46400 to C46700)	60.0 Cu, 39.25 Zn, 0.75 Sn	380–610	170–455	50–17	Aircraft turnbuckle barrels, balls, bolts, marine hardware, valve stems, condensor plates.

Copper and Copper Alloys

- **Best conductors of electricity and heat**

TABLE 3.10

Properties and Typical Applications of Various Wrought Bronzes

Type and UNS Number	Nominal Composition (%)	Ultimate Tensile Strength (MPa)	Yield Strength (MPa)	Elongation in 50 mm (%)	Typical Applications
Architectural bronze (C38500)	57.0 Cu, 3.0 Pb, 40.0 Zn	415	140 (as extruded)	30	Architectural extrusions, storefronts, thresholds, trim, butts, hinges.
Phosphor bronze, 5% A (C51000)	95.0 Cu, 5.0 Sn, trace P	325–960	130–550	64–2	Bellows, clutch disks, cotter pins, diaphragms, fasteners, wire brushes, chemical hardware, textile machinery.
Free-cutting phosphor bronze (C54400)	88.0 Cu, 4.0 Pb, 4.0 Zn, 4.0 Sn	300–520	130–435	50–15	Bearings, bushings, gears, pinions, shafts, thrust washers, valve parts.
Low-silicon bronze, B (C65100)	98.5 Cu, 1.5 Si	275–655	100–475	55–11	Hydraulic pressure lines, bolts, marine hardware, electrical conduits, heat-exchanger tubing.
Nickel–silver, 65–18 (C74500)	65.0 Cu, 17.0 Zn, 18.0 Ni	390–710	170–620	45–3	Rivets, screws, zippers, camera parts, base for silver plate, nameplates, etching stock.

Nickel and Nickel Alloys

- **High strength, toughness, corrosion resistance**

TABLE 3.11

Properties and Typical Applications of Various Nickel Alloys (All Alloy Names are Trade Names)

Alloy (Condition)	Principal Alloying Elements (%)	Ultimate Tensile Strength (MPa)	Yield Strength (MPa)	Elongation in 50 mm (%)	Typical Applications
Nickel 200 (annealed)	None	380–550	100–275	60–40	Chemical- and food-processing industry, aerospace equipment, electronic parts.
Duranickel 301 (age hardened)	4.4 Al, 0.6 Ti	1300	900	28	Springs, plastics-extrusion equipment, molds for glass, diaphragms.
Monel R-405 (hot rolled)	30 Cu	525	230	35	Screw-machine products, water-meter parts.
Monel K-500 (age hardened)	29 Cu, 3Al	1050	750	20	Pump shafts, valve stems, springs.
Inconel 600 (annealed)	15 Cr, 8 Fe	640	210	48	Gas-turbine parts, heat-treating equipment, electronic parts, nuclear reactors.
Hastelloy C-4 (solution treated and quenched)	16 Cr, 15 Mo	785	400	54	High-temperature stability, resistance to stress-corrosion cracking.

Superalloys

- **Heat resistance, high temperature**

TABLE 3.12

Properties and Typical Applications of Various Nickel-Base Superalloys at 870°C (1600°F) (All Alloy Names Are Trade Names)

Alloy	Condition	Ultimate Tensile Strength (MPa)	Yield Strength (MPa)	Elongation in 50 mm (%)	Typical Applications
Astroloy	Wrought	770	690	25	Forgings for high-temperature applications.
Hastelloy X	Wrought	255	180	50	Jet-engine sheet parts.
IN-100	Cast	885	695	6	Jet-engine blades and wheels.
IN-102	Wrought	215	200	110	Superheater and jet-engine parts.
Inconel 625	Wrought	285	275	125	Aircraft engines and structures, chemical-processing equipment.
Inconel 718	Wrought	340	330	88	Jet-engine and rocket parts.
MAR-M 200	Cast	840	760	4	Jet-engine blades.
MAR-M 432	Cast	730	605	8	Integrally cast turbine wheels.
René 41	Wrought	620	550	19	Jet-engine parts.
Udimet 700	Wrought	690	635	27	Jet-engine parts.
Waspaloy	Wrought	525	515	35	Jet-engine parts.

Titanium and Titanium Alloys

- **High strength-to-weight ratio, corrosion resistance**

TABLE 3.13

Properties and Typical Applications of Wrought Titanium Alloys

			Room Temperature				Various Temperatures					
Nominal Composition (%)	UNS	Condition	Ultimate Tensile Strength (MPa)	Yield Strength (MPa)	Elongation (%)	Reduction of Area (%)	Temp (°C)	Ultimate Tensile Strength (MPa)	Yield Strength (MPa)	Elongation (%)	Reduction of Area (%)	Typical Applications
99.5 Ti	R50250	Annealed	330	240	30	55	300	150	95	32	80	Airframes; chemical, desalination, and marine parts; plate-type heat exchangers.
5 Al, 2.5 Sn	R54520	Annealed	860	810	16	40	300	565	450	18	45	Aircraft-engine compressor blades and ducting; steam-turbine blades.
6 Al, 4 V	R56400	Annealed	1000	925	14	30	300	725	650	14	35	Rocket motor cases; blades and disks for aircraft turbines and compressors; orthopedic implants; structural forgings; fasteners.
							425	670	570	18	40	
							550	530	430	35	50	
		Solution + age	1175	1100	10	20	300	980	900	10	28	
13 V, 11 Cr, 3 Al	R58010	Solution + age	1275	1210	8	–	425	1100	830	12	–	High-strength fasteners; aerospace components; honeycomb panels.

High/Low Melting Temperature

- **Refractory metals**
  - Molybdenum
  - Niobium
  - Tungsten
  - Tantalum

- **Low melting point metals**
  - Lead
  - Zinc
  - Tin

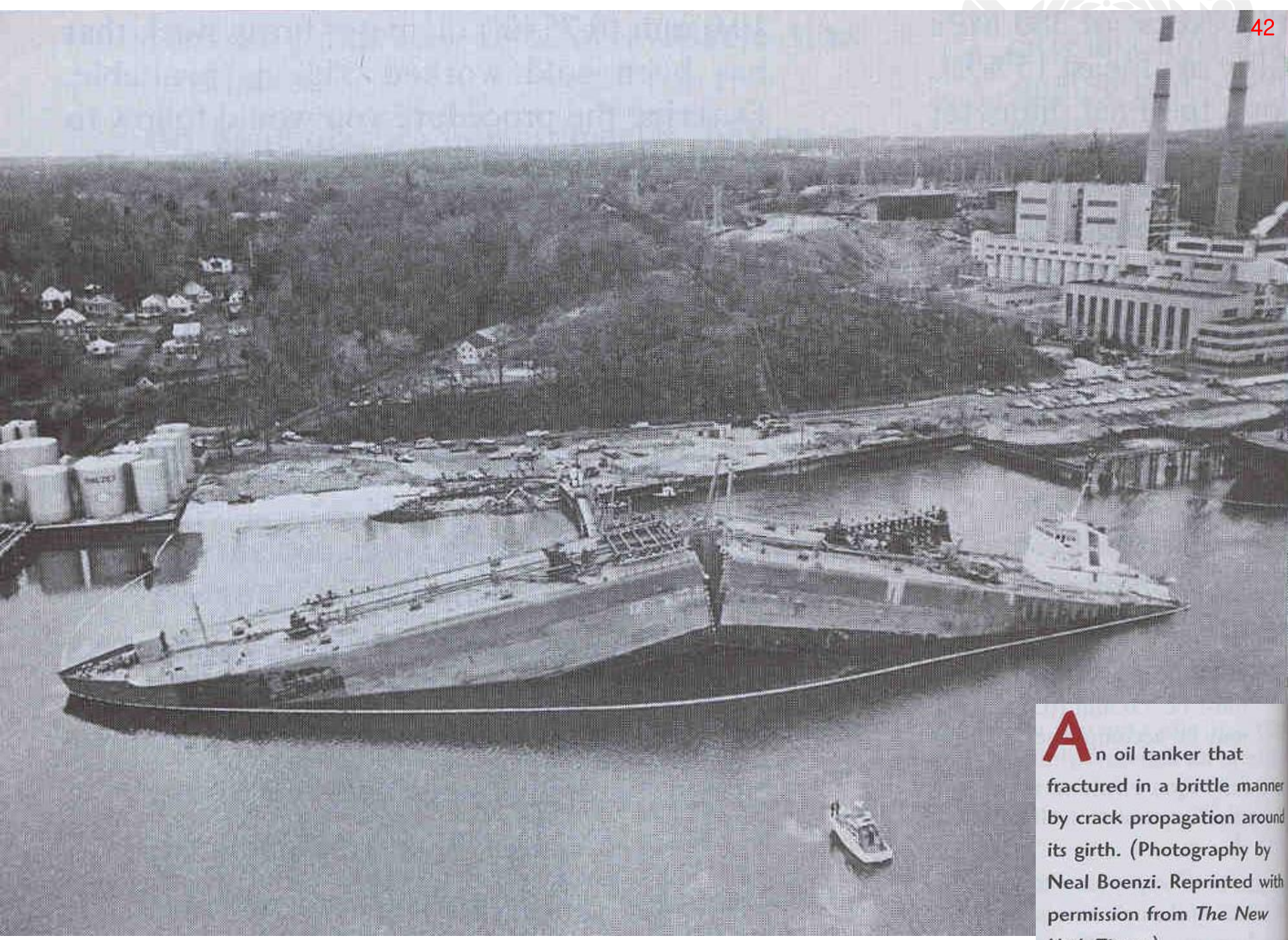

An oil tanker that fractured in a brittle manner by crack propagation around its girth. (Photography by Neal Boenzi. Reprinted with permission from *The New York Times*.)

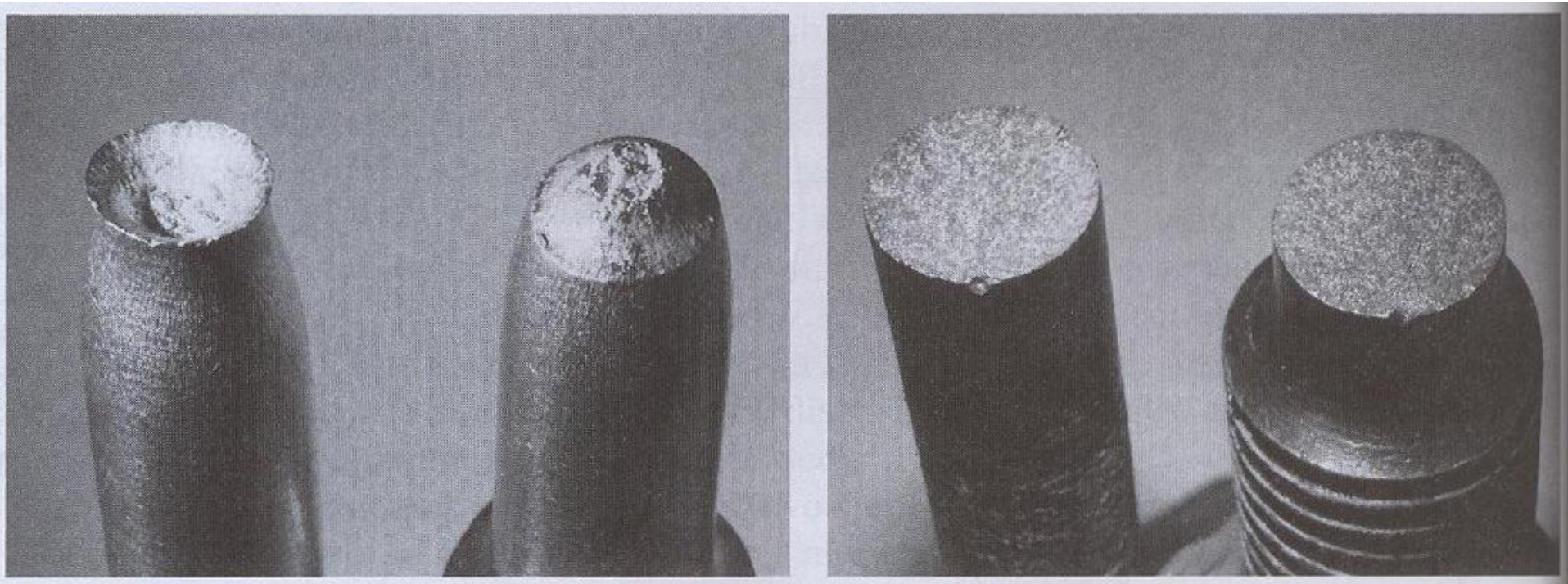

(a) (b)

Figure 9.3 (*a*) Cup-and-cone fracture in aluminum. (*b*) Brittle fracture in a mild steel.

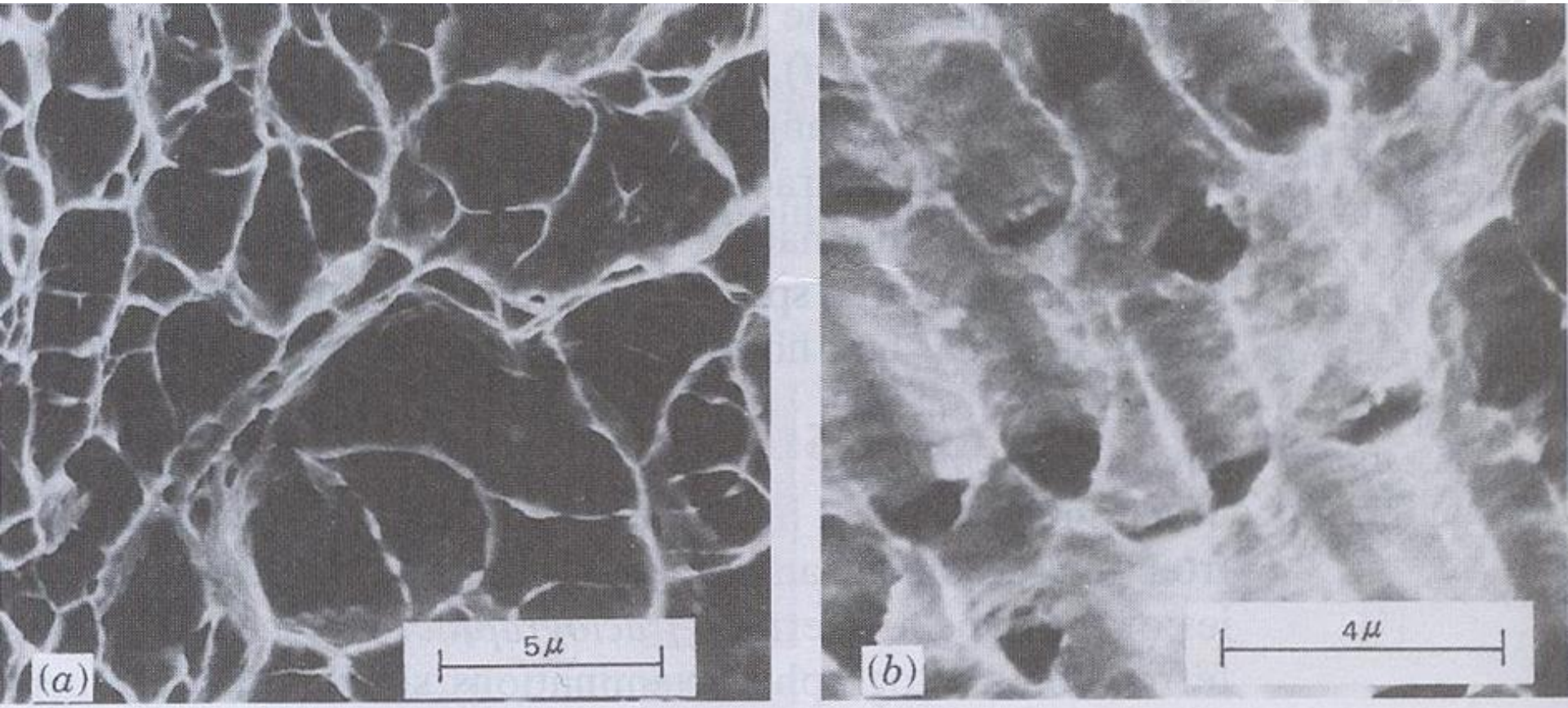

Figure 9.4 (*a*) Scanning electron fractograph showing spherical dimples characteristic of ductile fracture resulting from uniaxial tensile loads. 3300×. (*b*) Scanning electron fractograph showing parabolic-shaped dimples characteristic of ductile fracture resulting from shear loading. 5000×. (From R. W. Hertzberg, *Deformation and Fracture Mechanics of Engineering Materials,* 3rd edition. Copyright © 1989 by John Wiley & Sons, New York. Reprinted by permission of John Wiley & Sons, Inc.)

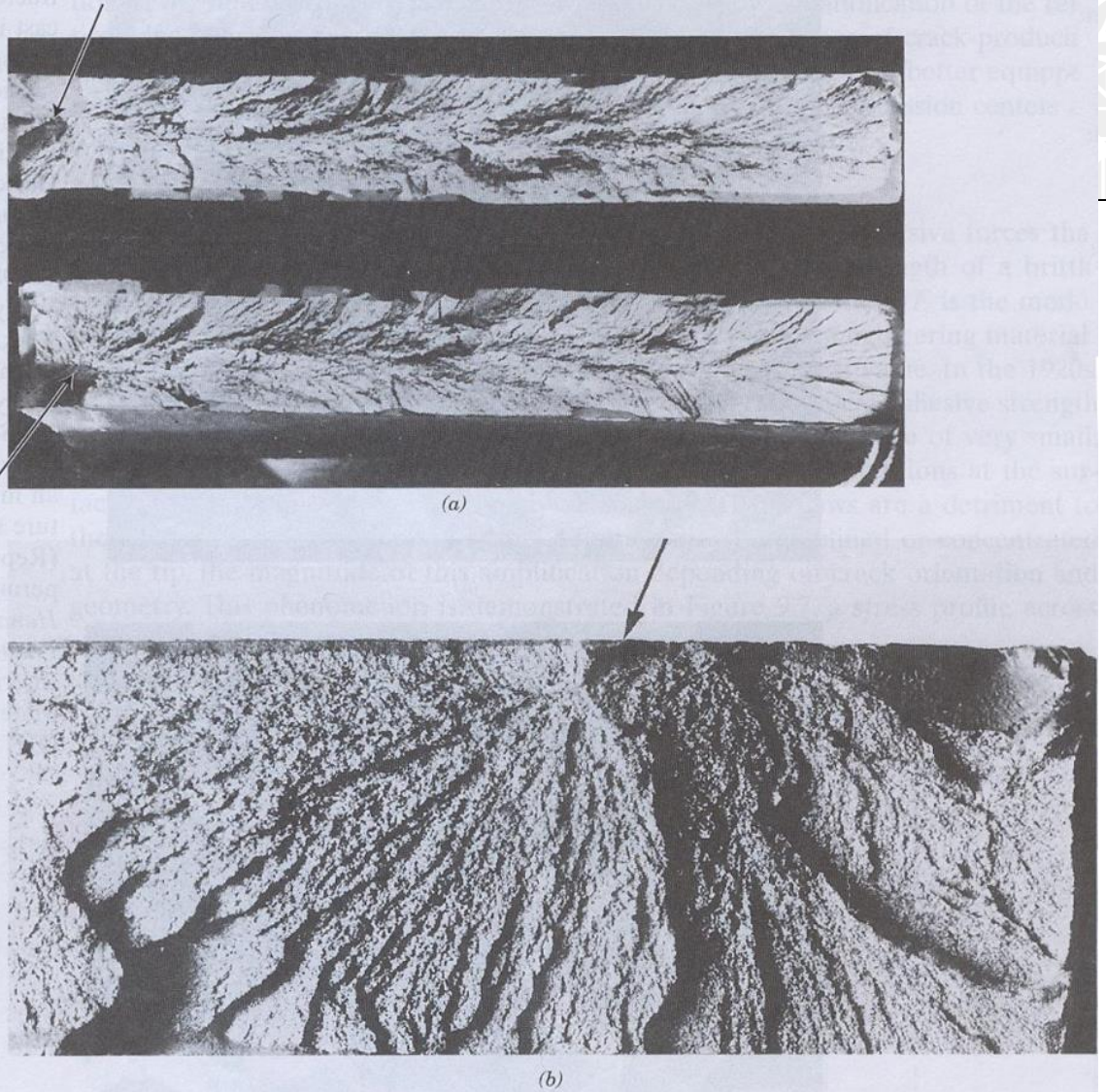

(a)

(b)

Figure 9.5 (*a*) Photograph showing V-shaped "chevron" markings characteristic of brittle fracture. Arrows indicate origin of crack. Approximately actual size. (From R. W. Hertzberg, *Deformation and Fracture Mechanics of Engineering Materials,* 3rd edition. Copyright © 1989 by John Wiley & Sons, New York. Reprinted by permission of John Wiley & Sons, Inc. Photograph courtesy of Roger Slutter, Lehigh University.) (*b*) Photograph of a brittle fracture surface showing radial fan-shaped ridges. Arrow indicates origin of crack. Approximately 2×. (Reproduced with permission from D. J. Wulpi, *Understanding How Components Fail,* American Society for Metals, Materials Park, OH, 1985.)

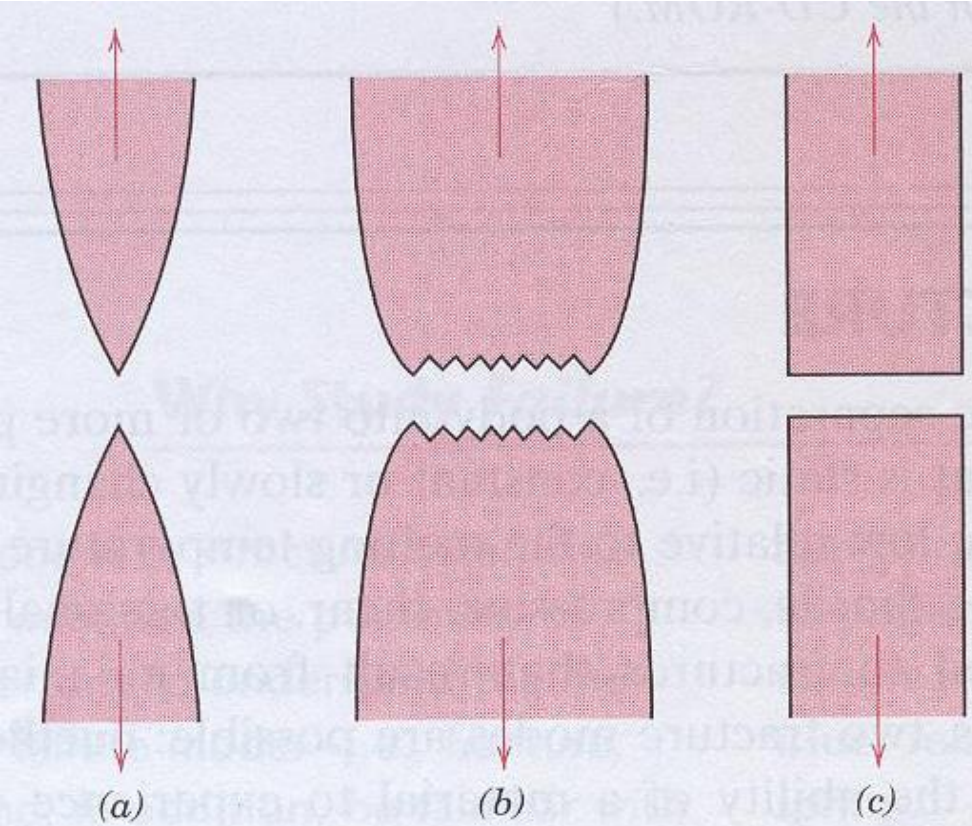

Figure 9.1 (*a*) Highly ductile fracture in which the specimen necks down to a point. (*b*) Moderately ductile fracture after some necking. (*c*) Brittle fracture without any plastic deformation.

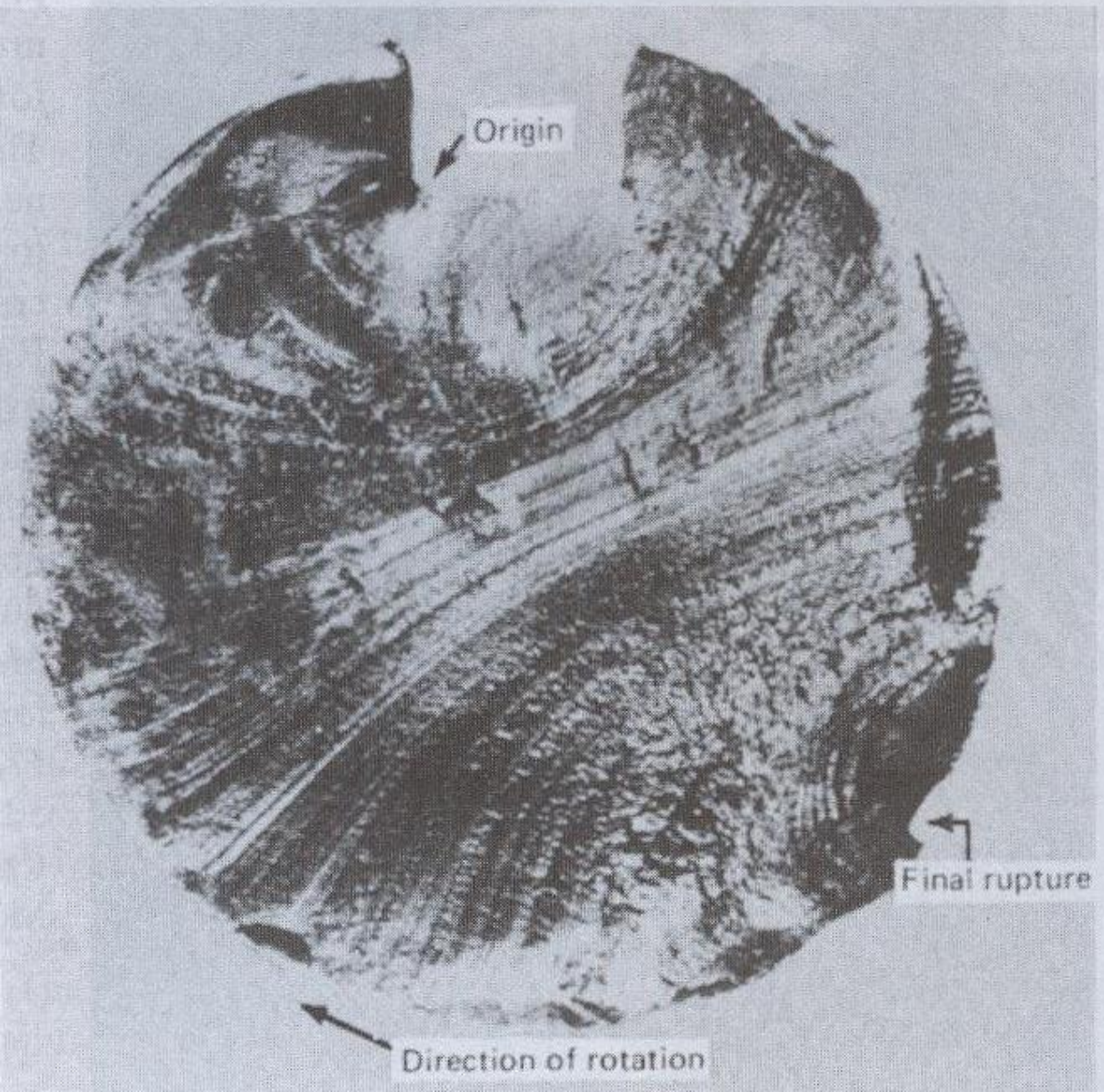

Figure 9.34 Fracture surface of a rotating steel shaft that experienced fatigue failure. Beachmark ridges are visible in the photograph. (Reproduced with permission from D. J. Wulpi, *Understanding How Components Fail,* American Society for Metals, Materials Park, OH, 1985.)

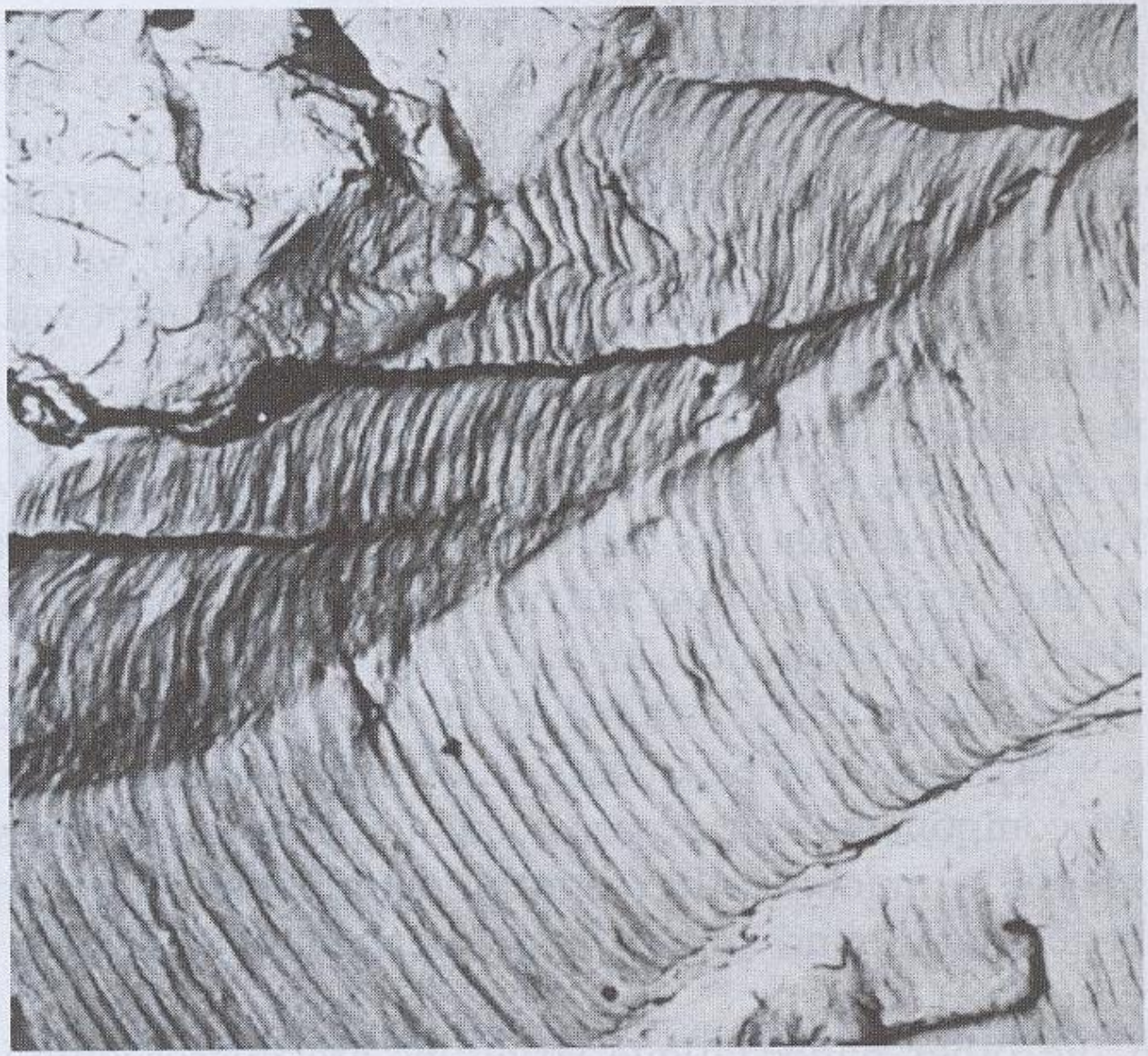

Figure 9.35 Transmission electron fractograph showing fatigue striations in aluminum. Magnification unknown. (From V. J. Colangelo and F. A. Heiser, *Analysis of Metallurgical Failures,* 2nd edition. Copyright © 1987 by John Wiley & Sons, New York. Reprinted by permission of John Wiley & Sons, Inc.)

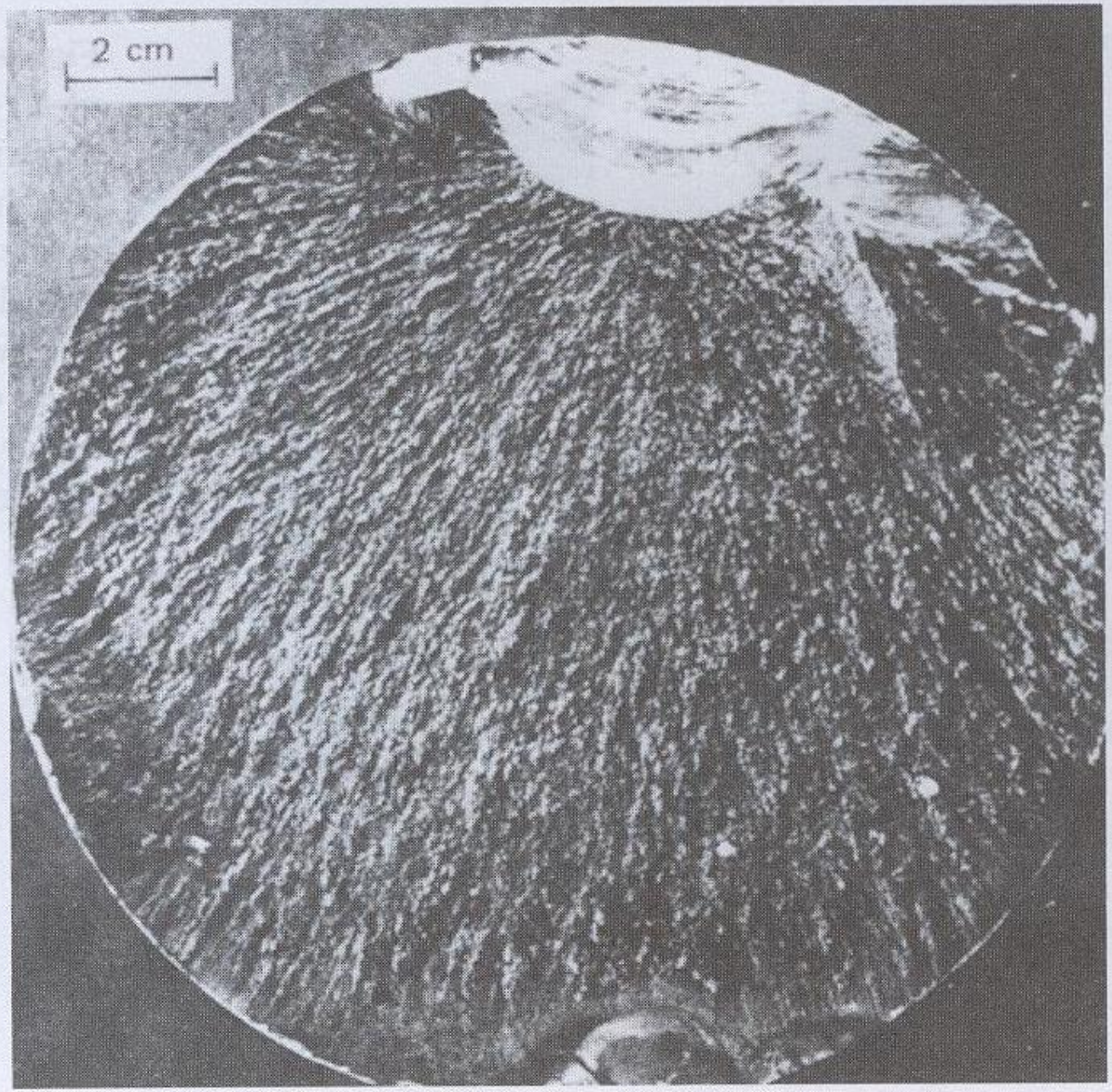

Figure 9.36 Fatigue failure surface. A crack formed at the top edge. The smooth region also near the top corresponds to the area over which the crack propagated slowly. Rapid failure occurred over the area having a dull and fibrous texture (the largest area). Approximately 0.5×. (Reproduced by permission from *Metals Handbook: Fractography and Atlas of Fractographs,* Vol. 9, 8th edition, H. E. Boyer, Editor, American Society for Metals, 1974.)

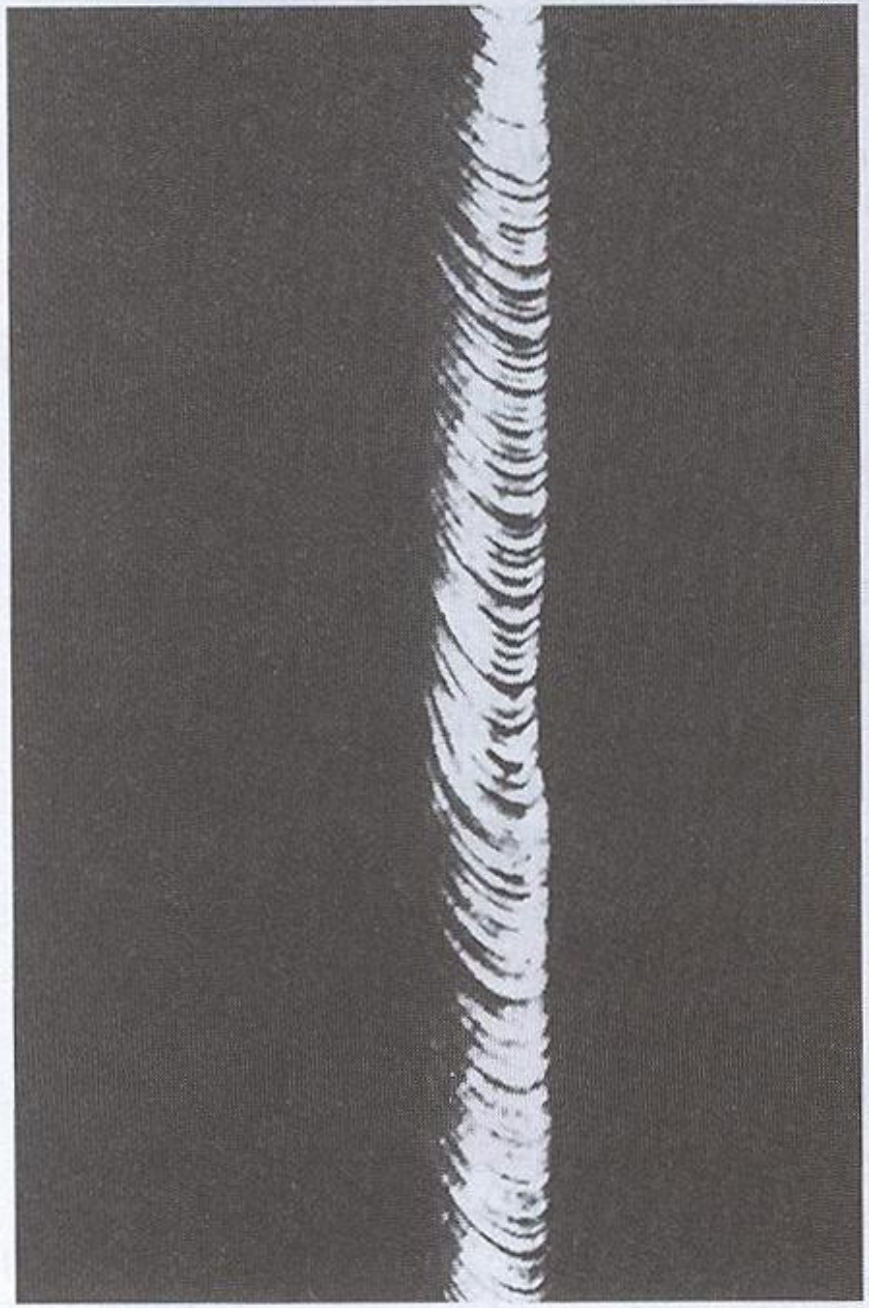

Figure 8.9 Slip in a zinc single crystal. (From C. F. Elam, *The Distortion of Metal Crystals,* Oxford University Press, London, 1935.)

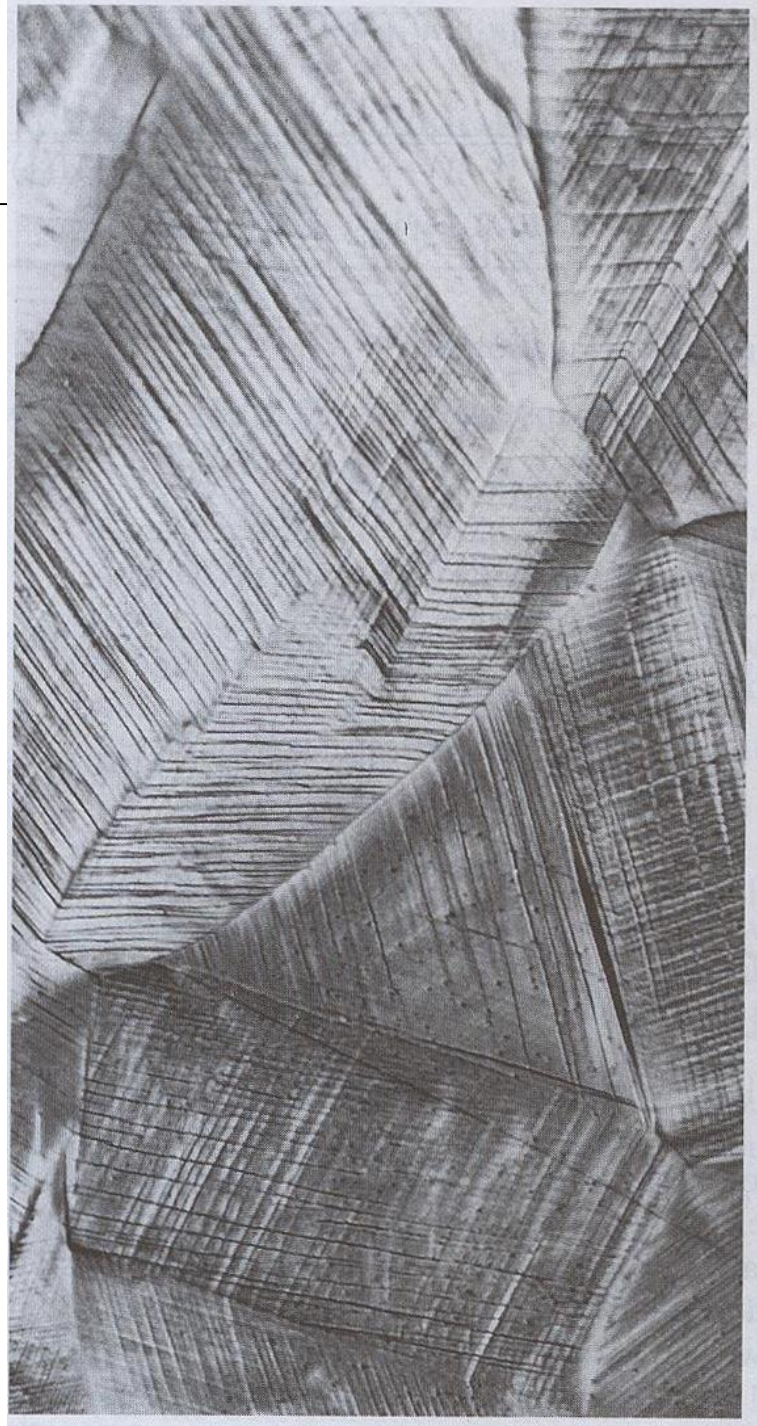

Figure 8.10 Slip lines on the surface of a polycrystalline specimen of copper that was polished and subsequently deformed. 173×. [Photomicrograph courtesy of C. Brady, National Bureau of Standards, Washington, DC (now the National Institute of Standards and Technology, Gaithersburg, MD).]

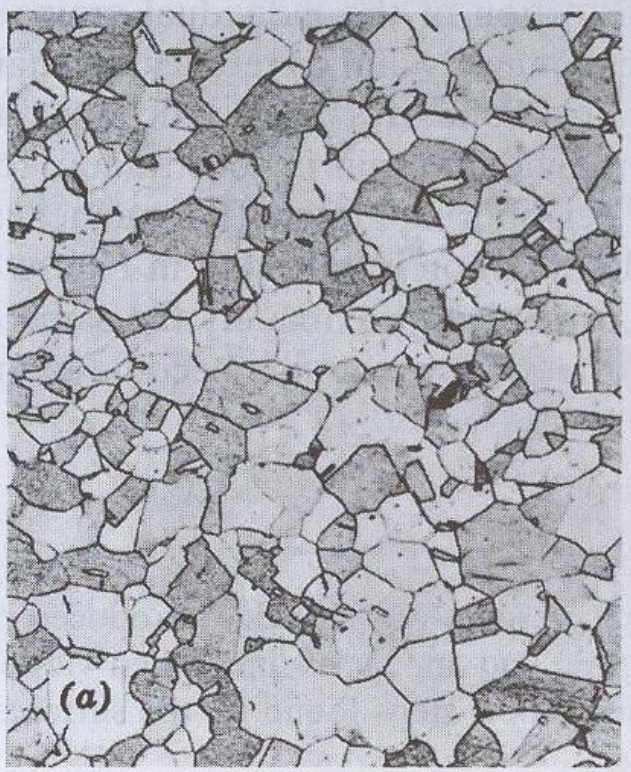

Figure 8.11 Alteration of the grain structure of a polycrystalline metal as a result of plastic deformation. (*a*) Before deformation the grains are equiaxed. (*b*) The deformation has produced elongated grains. 170×. (From W. G. Moffatt, G. W. Pearsall, and J. Wulff, *The Structure and Properties of Materials,* Vol. I, *Structure,* p. 140. Copyright © 1964 by John Wiley & Sons, New York. Reprinted by permission of John Wiley & Sons, Inc.)

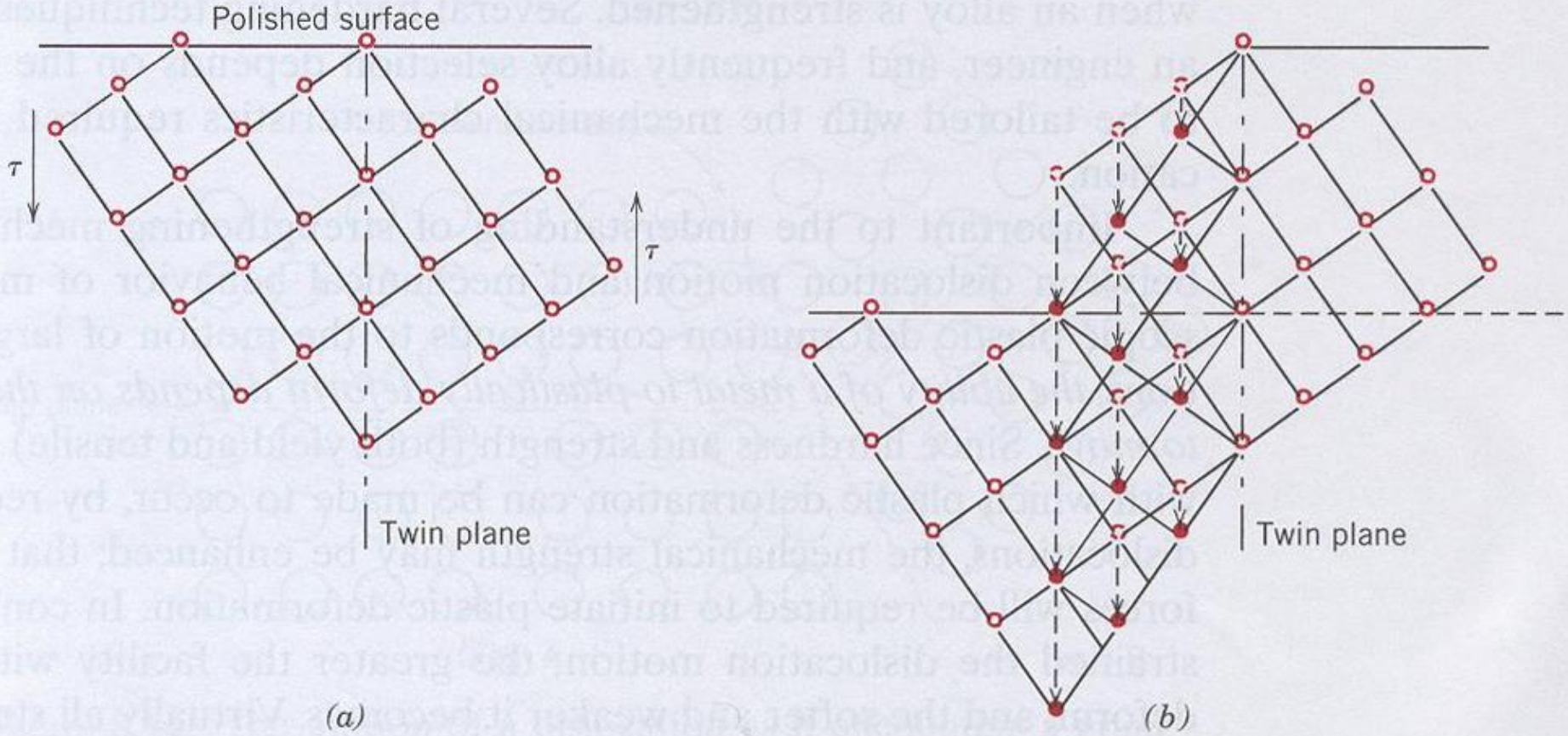

Figure 8.12 Schematic diagram showing how twinning results from an applied shear stress τ. In (*b*), open circles represent atoms that did not change position; dashed and solid circles represent original and final atom positions, respectively. (From G. E. Dieter, *Mechanical Metallurgy,* 3rd edition. Copyright © 1986 by McGraw-Hill Book Company, New York. Reproduced with permission of McGraw-Hill Book Company.)

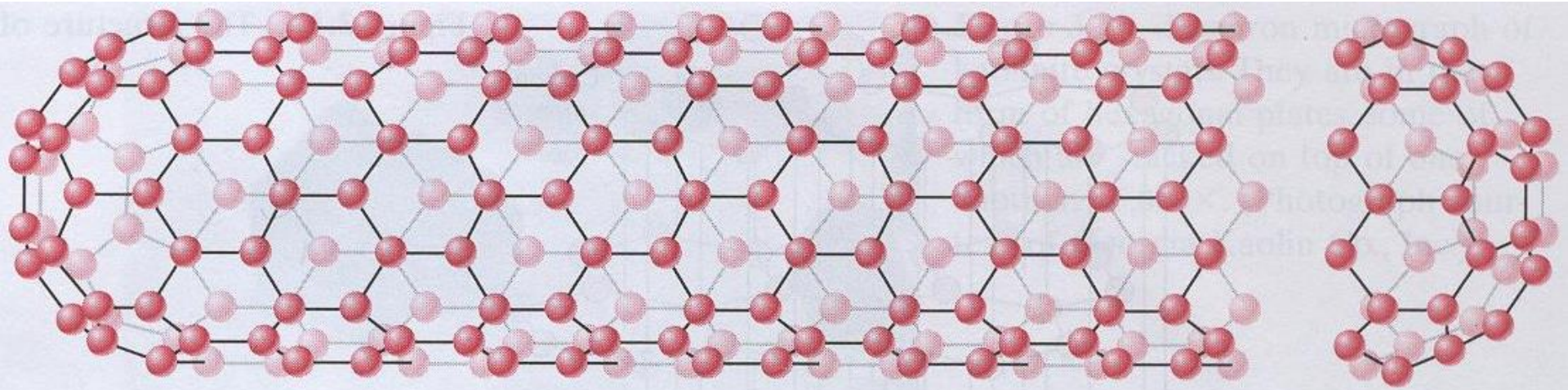

Figure 3.19 The structure of a carbon nanotube. (Reprinted by permission from *American Scientist*, magazine of Sigma Xi, The Scientific Research Society. Illustration by Aaron Cox/*American Scientist*.)

- **Young's Modulus 1~1.2TPa**
- **Shear Modulus of CNT: 0.41~1TPa**
- **Strength of CNT: 10~63GPa**

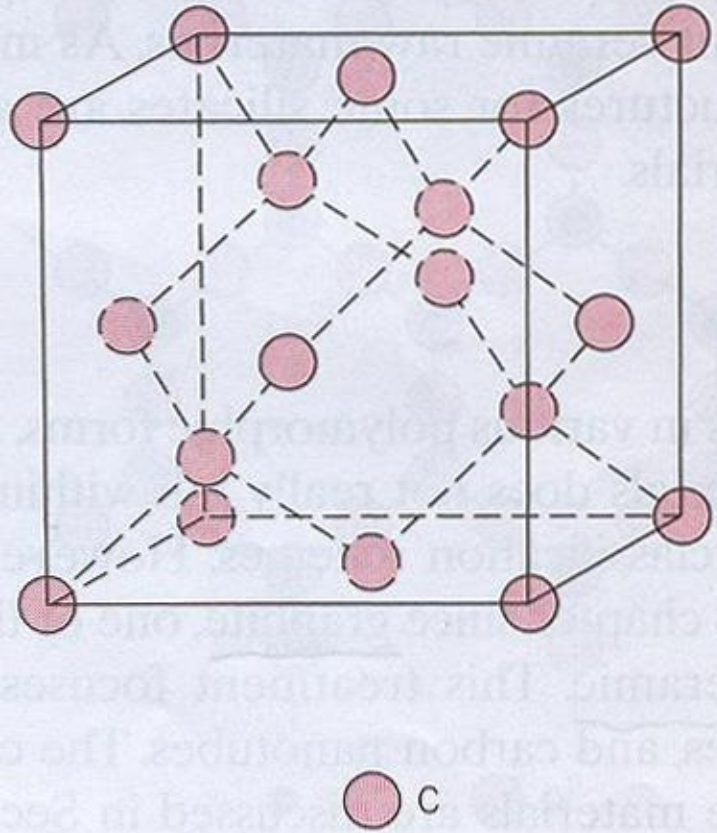

Figure 3.16 A unit cell for the diamond cubic crystal structure.

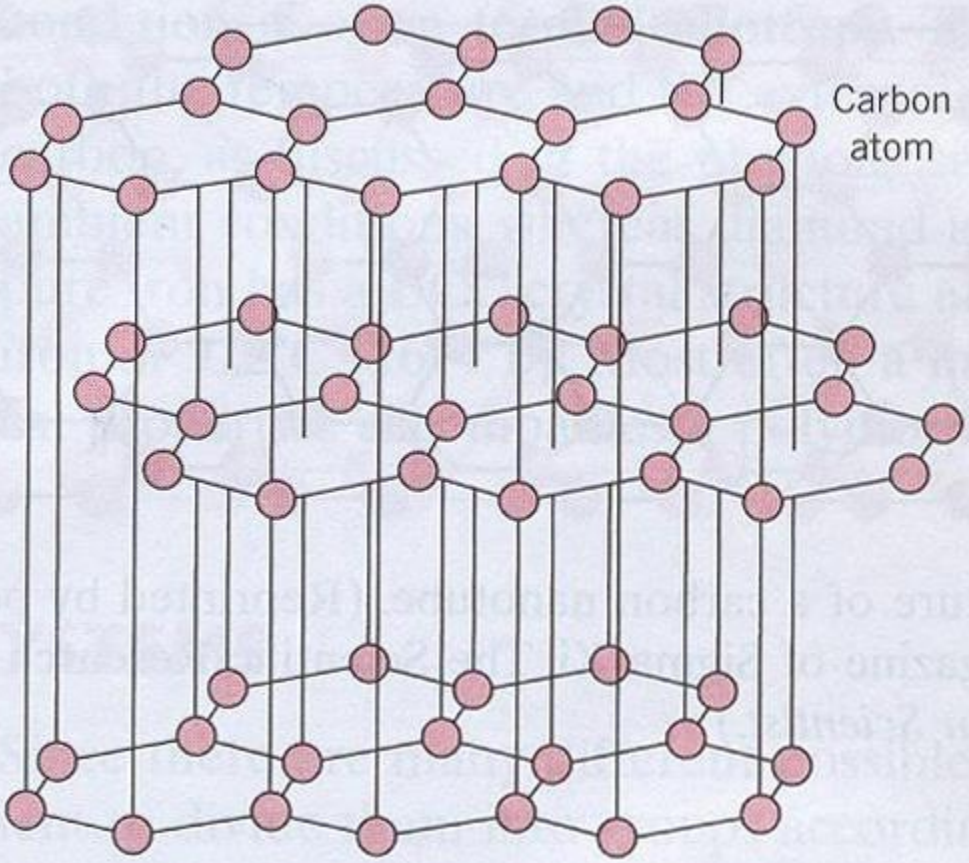

Figure 3.17 The structure of graphite.

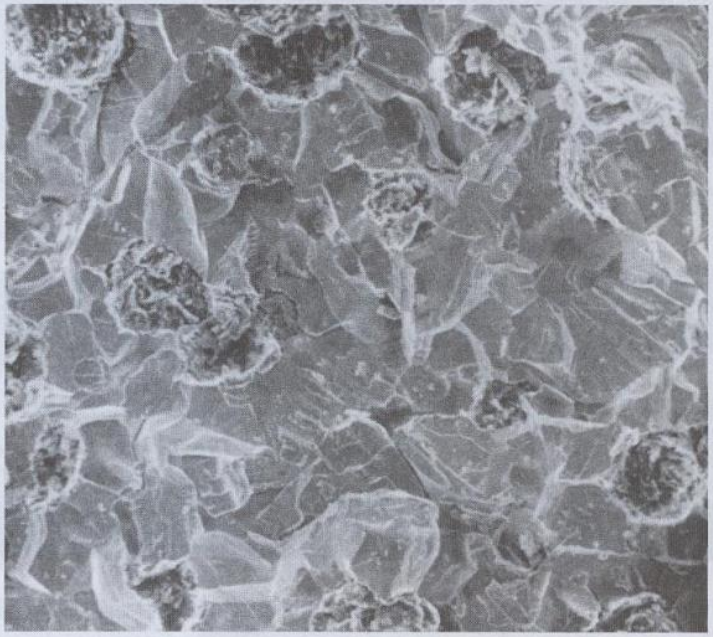

(a)

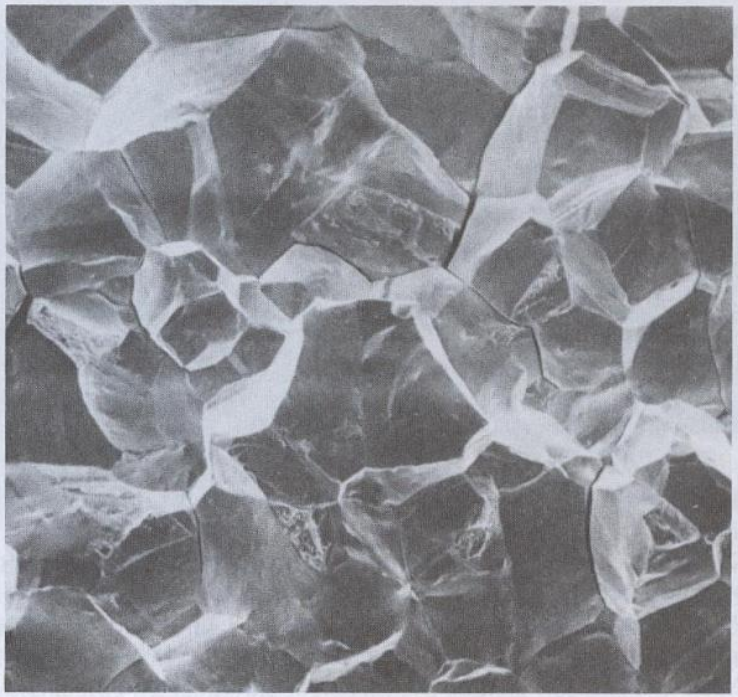

(b)

Figure 9.6 (*a*) Scanning electron fractograph of ductile cast iron showing a transgranular fracture surface. Magnification unknown. (From V. J. Colangelo and F. A. Heiser, *Analysis of Metallurgical Failures*, 2nd edition. Copyright © 1987 by John Wiley & Sons, New York. Reprinted by permission of John Wiley & Sons, Inc.) (*b*) Scanning electron fractograph showing an intergranular fracture surface. 50×. (Reproduced with permission from *ASM Handbook*, Vol. 12, *Fractography*, ASM International, Materials Park, OH, 1987.)

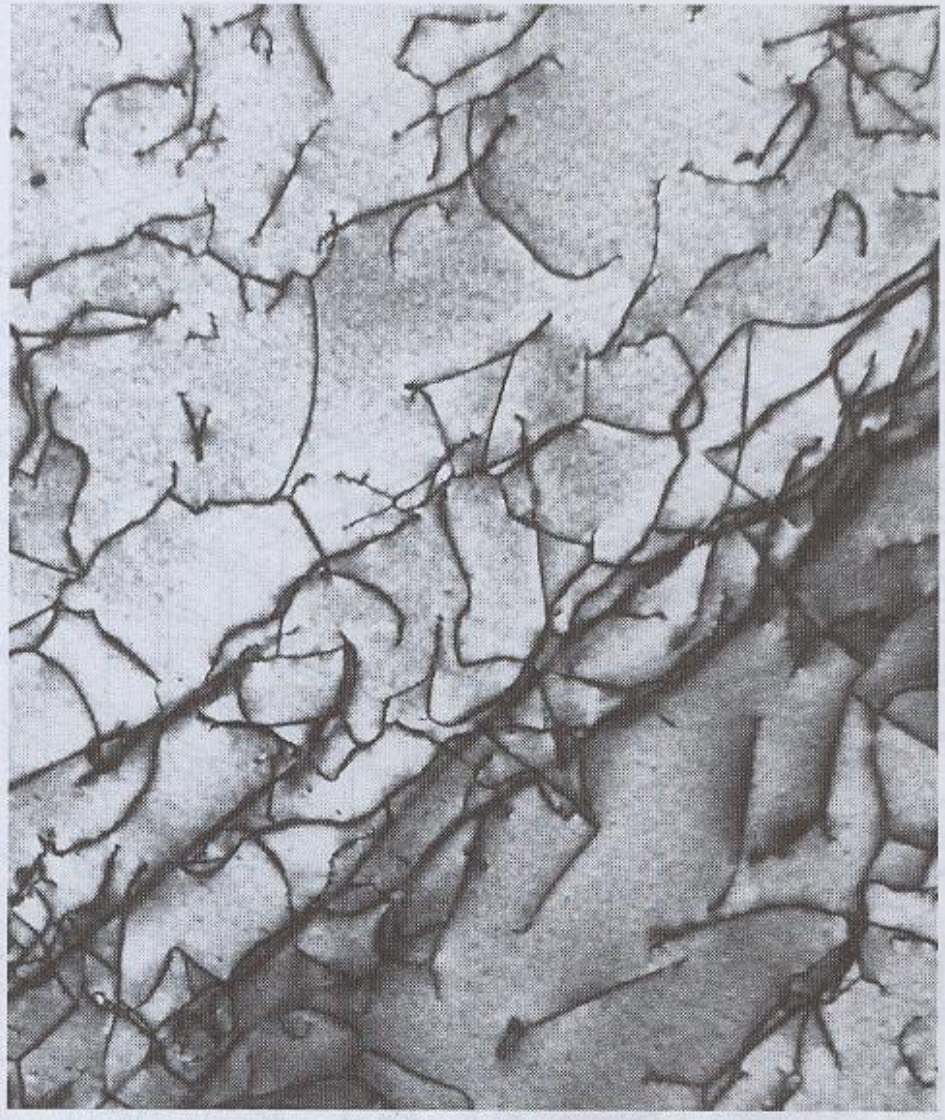

Figure 5.10 A transmission electron micrograph of a titanium alloy in which the dark lines are dislocations. 51,450×. (Courtesy of M. R. Plichta, Michigan Technological University.)